1

Introduction

1.1 Definition of Glassy States

A "glassy or vitreous" state is classified as a state of condensed matter in which there is a clear absence of a three-dimensional periodic structure. The periodicity is defined by the repetition of point groups (e.g. atoms or ions) occupying sites in the structure, following a crystallographic symmetry, namely, the mirror, inversion and rotation. A glass is a condensed matter exhibiting elasticity below a phase transition temperature, known as the glass transition temperature, which is designated in this text as (T_g). By comparison, an "amorphous" state, as in the "vitreous" state, has an all-pervasive lack of three-dimensional periodicity; it is more comparable with a liquid rather than a solid. An amorphous structure lacks elasticity and has a propensity to flow under its own weight more readily than a solid-like vitreous state does below T_g. *An amorphous inorganic film also has a glass transition temperature and elastic behaviour, which varies with that of the corresponding vitreous state of the same material*. The recognition of apparent differences in the properties of "vitreous" and "amorphous" structures, will be discussed in subsequent chapters on fabrication and processing and such comparative characterizations are essential in developing a deeper understanding of a structure–optical and spectroscopic properties of transparent "inorganic glasses as photonic materials" for guiding photons and their interactions with the medium. Such differences in structural and thermal properties between a glassy or amorphous and a crystalline state explain why the disordered materials demonstrate unique physical, thermo-mechanical, optical and spectroscopic properties, facilitating light confinement and propagation for long-haul distances better than any other condensed matter.

1.2 The Glassy State and Glass Transition Temperature (T_g)

The liquid-to-solid phase transition at the melting point (T_f) of a solid, for example, is characterized as a thermodynamically reversible or an equilibrium transition point, at which both the liquid and solid phases co-exist. Since at the melting point both phases are in equilibrium, the resulting Gibbs energy change (ΔG^f), as shown in Equation 1.1, of the phase

Inorganic Glasses for Photonics – Fundamentals, Engineering and Applications, First Edition. Animesh Jha.

transition is zero, which then helps in defining the net entropy change associated with the phase change at T_f:

$$\Delta G^f = \Delta H^f - T_f \Delta S^f = 0 \tag{1.1}$$

In Equation 1.1, ΔH^f and ΔS^f are the enthalpy and entropy changes at the melting point. Since ΔG^f equates to a zero value at T_f, from Equation 1.1, the entropy change at T_f consequently is equal to:

$$\Delta S^f = \frac{\Delta H^f}{T_f} \tag{1.2a}$$

From Equation 1.2a, for pure solids the magnitude of entropic disorder can thus be determined at the melting point by measuring the enthalpy of fusion. This characteristic of a solid–liquid transition will become quite relevant in the examination of glass-formation in multicomponent systems. In Figure 1.1, the liquid-to-crystal and liquid-to-glass transitions are shown by identifying the T_f and a range of transition temperatures, T_g^1, T_g^2 and T_g^3, respectively. These glass transition temperatures are dependent on the quenching paths AA_1E, AA_2F and AA_3G, which differ from the equilibrium route ABCD for liquid-crystal transition at T_f.

In Figure 1.1, the glass experiencing the fastest quenching rate (Q_3) has the corresponding transition temperature at T_g^3, whereas the quenching rates Q_2 and Q_1 yield glasses having transition temperature at T_g^2 and T_g^1, respectively. The end entropic points thus relate to the thermal history of each glass. The slowest cooling rate yields the lowest temperature, as the supercooled liquid state below T_f attains a metastable thermodynamic state, which is

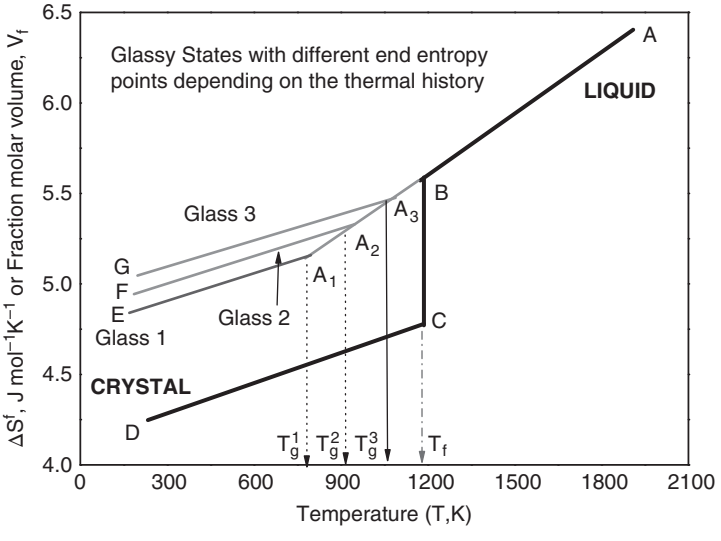

Figure 1.1 *Plot of the entropy change (ΔS^f in J mol^{-1} K^{-1}) in a solid–liquid and liquid-glassy state transitions, shown schematically to illustrate the respective apparent change in the value of entropy end point, as a result of various quench rates applied, which are designated by the paths AA_1E, AA_2F, and AA_3G.*

still higher in Gibbs energy than the equilibrium crystalline state designated by line CD in Figure 1.1. When the fastest quenching rate path, AA_3G, is followed the liquid has little time to achieve the thermodynamic equilibrium, as reflected by the transition temperature T_g^3, which is closest to the melting point.

The annealing of the fastest quenched glass in Figure 1.1, having a transition temperature at T_g^3, provides the driving force for structural relaxation to lower energy states progressively. With a prolonged isothermal annealing, the end point entropy state might eventually reach much closer to the equilibrium crystalline state (line CD in Figure 1.1). As the annealing allows the quenched glass to dissipate most of the energy in a metastable quenched state, the end point entropy never approaches the line CD, which is consistent with the theory proposed by Boltzmann in the context of the second law of thermodynamics. This condition mathematically limits the value of viscosity approaching infinity, an impossible value. Considering the thermodynamic state properties, e.g. the molar volume (V) and entropy (S), and their dependence on pressure (P) and temperature (T), any change in the entropy of a state corresponds to a proportional change in the molar volume, which follows from the differentials in Equations 1.2b–d, shown below. It is for this reason that in Figure 1.1 the discontinuity in fractional change in molar free volume (v_f), which is dependent on V, is shown along with the entropy change:

$$dG = -SdT + VdP \tag{1.2b}$$

$$\left[\frac{\partial G}{\partial T}\right]_P = -S \tag{1.2c}$$

$$\left[\frac{\partial G}{\partial P}\right]_T = +V \tag{1.2d}$$

The implication of thermodynamic state analysis in Equations 1.2b–d is that the discontinuities in glassy states are also observed when their state properties, such as the enthalpy (H), specific heats at constant pressure (C_p) and volume (C_v), thermal expansion coefficient (α_V) and isothermal compressibility (β_T), are plotted against temperature. Discontinuities in the thermodynamic state properties for several glass-forming liquids are compared and discussed by Paul [1] and Wong and Angell [2] in publications that readers may find helpful.

From Figure 1.1, the glass transition temperature is represented by the presence of a discontinuity, which is dependent on the quenching rate (Q_i), and the points representing T_gs are not sharp or abrupt, as shown in the liquid-to-crystal transition. The range of T_gs in Figure 1.1 is characterized as the "*fictive glass temperature*" and their position is dependent on the quenching history. Several text books designate the fictive temperature as T_f, and readers should cautiously interpret this temperature along with the quench rate and associated thermal history, because unlike T_f, the T_gs are not fixed phase transition points. A major discrepancy in the property characterization might arise if experiments are not carefully designed to study the sub-T_g and above-T_g structural relaxation phenomena, which are discussed in great detail by Varsheneya [3a] in his text book. Elliott [4] explains the exponential relationship between quenching rate and T_g in Equation 1.3, showing that the corresponding relaxation time (which is the inverse of the quenching rate) is likely to be imperceptibly long, since a glass is annealed to achieve a new metastable equilibrium

state above a crystalline phase, corresponding to line CD in Figure 1.1:

$$Q_i = Q_o \exp\left[-B\left\{\frac{1}{T_g} - \frac{1}{T_f}\right\}\right] \tag{1.3}$$

In Equation 1.3, the value of Q_o for different glasses differs, as observed by Owen [5], and was found to be of the order of 10^{23} and $10^4\,K\,s^{-1}$ between Se and As_2S_3 glasses. The constant B was found to be of the order of 3×10^{-5} K. An analysis of quenching rate and glass transition temperature implies that near T_g, there is an Arrhenius type activation energy barrier, which is path dependent and can be reached in numerous ways by following different thermal histories, which is discussed extensively by Varsheneya [3b]. Based on path dependence analysis and the associated changes in the first order thermodynamic properties, namely the enthalpy of glass transition, the phase transition is a "first-order" transition and, unlike the Curie temperature in a magnetic metallic glass, the glass transition is not a second-order transition. The Curie temperature is a fixed point, dependent upon the electronic-spin relaxation, the time-scale for which is of the order of 10^{-15} (femto to sub-femto) seconds, which is six orders of magnitude faster than the molecular relaxation characterized by an Arrhenius type of energy barrier. From reaction rate theory, the pre-exponential in the rate equation is equal to k_BT/h, where k_B and h are the Boltzmann constant and Planck's constant, respectively and T is the absolute temperature. Applying the reaction rate theory for quenching of a glass, the minimum and maximum values therefore may vary between 10^{-7} and 10^{-9} s, which leads to an interesting discussion on the interaction of ultrafast lasers (pico- and femtosecond) with a glass and consequential structural changes. It is therefore not unreasonable to expect a dramatic change in the relaxation properties of glassy thin films formed in a femtosecond quenching regime when compared with the same composition glass produced via splat ($10^6\,K\,s^{-1}$) and air quenching ($10^2\,K\,s^{-1}$) techniques. Such a large difference in the magnitude of quenching glass is likely to yield structural variations (molar volume, expansion coefficients, refractive index, electronic edge), which may then be manifested in the corresponding relaxation rate, in accordance with Equation 1.3

1.3 Kauzmann Paradox and Negative Change in Entropy

There has been continued debate on the Kauzmann paradox in the glass literature, in relation to the path dependence of quenching of glass-forming liquids and the attainment of an overall entropy state that is lower than that of the crystalline state (line CD in Figure 1.1), which implies that the glass attains a negative entropic state. Based on the entropy change in supercooled glycerol, reported earlier by Jäckle [6] in Figure 1.2, Kauzmann's data [7] were critically analysed by Varsheneya [3b], who explained that the laws of thermodynamics are not exempt within the concept of the "Kauzmann paradox".

In supercooled liquids the structural arrangements are so rapid that the resultant changes cannot be depicted on the time-scale of measurements. There is, though, a further argument that continues to support the nature of thermodynamic laws that the entropy change in a "system" may be negative. However, the "total or universe" entropic change is a sum of the entropies of a "system" and its "surrounding". Two examples are characterized herein to make an important point on the negative nature of entropy. The solidification point of quartz is

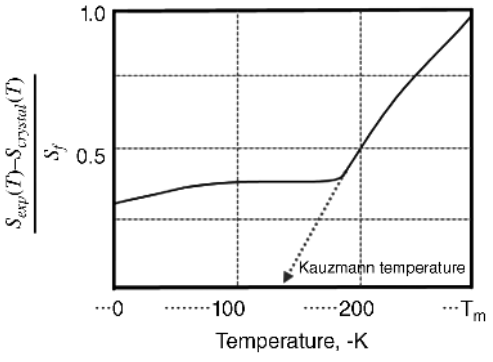

Figure 1.2 *Entropy change with respect to the melting point entropy against temperature, extrapolated to determine the Kauzmann temperature (T_k) after Jäckle [6]. Source: J. Jackel 1986. Reproduced with permission from Elsevier.*

2273 K, and the entropy of fusion $(\Delta S^{\mathrm{f}})_{\mathrm{System}}$, from Equation 1.2a, is $-4.52\,\mathrm{J\,mol^{-1}\,K^{-1}}$, yielding an enthalpy ($\Delta H^{\mathrm{f}}$) of solidification that is equal to $-10278\,\mathrm{J\,mol^{-1}}$. Since there is only a small difference in the entropies of crystalline quartz, liquid silica and the glassy states, with a comparable value of around $4.52\,\mathrm{J\,mol^{-1}\,K^{-1}}$, during quenching as the liquid is solidifying to a lower volume state the sign of entropy "changes to a negative" value below the melting point, indicating more structural order than in the liquid state above its melting point, which is consistent with Equation 1.1. The enthalpy released into the surrounding at 300 K, which is absorbing the heat (δQ), is $+10278\,\mathrm{J\,mol^{-1}}$ and therefore the corresponding entropy change in the surrounding $(\Delta S)_{\mathrm{Surrounding}}$, from the second law of thermodynamics, is equal to:

$$\frac{\delta Q}{T_{\mathrm{Surrounding}}} = \frac{+10278}{300} = +34.26\,\mathrm{J\,mol^{-1}\,K^{-1}}$$

which yields a net change in entropy of the universe that is equal to $+29.74\,\mathrm{J\,mol^{-1}\,K^{-1}}$. The formation of a layer of amorphous alumina via the reaction:

$$2\mathrm{Al(solid)} + \tfrac{3}{2}\mathrm{O_2(gas)} = \mathrm{Al_2O_3(solid)}$$

over the surface of aluminium follows an identical argument because of the exothermic nature of the enthalpy of formation of alumina, which is $-1.8046 \times 10^6\,\mathrm{J\,mol^{-1}}$ of alumina and the corresponding negative value of entropy change is nearly $-132\,\mathrm{J\,mol^{-1}\,K^{-1}}$. For an endothermic reaction, the signs will reverse and the argument still holds, implying that the "exemption from the universal thermodynamic laws" is "impossible" in a physical phenomenon. The irreversible and path-dependent nature of metastable glassy states beautifully follows the laws of thermodynamics, irrespective of the route by which a glass or an amorphous state is achieved, namely via the quenching, sol–gel, pulsed laser deposition and mechanical grinding techniques.

1.4 Glass-Forming Characteristics and Thermodynamic Properties

In Table 1.1 we compare the enthalpy, entropy, melting and glass transition points for several glass-forming unary compounds. This comparative exercise of melting, glass-transition and thermodynamic properties at T_{f} will help us in identifying an important structural feature,

Table 1.1 *Comparison of the thermodynamic state properties, enthalpy (ΔH^f, J mol^{-1}), lattice energy (ΔH_{lat} kJ mol^{-1}) and entropy (ΔS^f, in eu), and melting points (T_f, K) of glass-forming compounds and their glass transition temperatures (T_g, K) [4,8,9].*

Unary compound	T_f (K)	ΔH^f (J mol^{-1})	ΔS^f (eu)	T_g (K)	Ratio T_g/T_f	ΔH_{lat} (kJ)
Silica (SiO_2)	1996	7700–10 880	1.08–1.30	1453	0.73	−911
Beryllium fluoride (BeF_2)	825	4750	1.37	598	0.73	−1028
Germanium oxide (GeO_2)	1388	8140	1.4	853	0.61	−580
Boric oxide (B_2O_3)	723	22 180–24 060	7.33–7.95	530	0.73	−1272
Zinc chloride ($ZnCl_2$)	591	10250	4.14	380	0.64	−415
Sulfur (S)	388	1720	4.14	246	0.63	—
Selenium (Se)	494	5860	2.83	318	0.64	—
Arsenic trisulfide (As_2S_3)	585	28675	11.71	478	0.82	−168
Arsenic triselenide (As_2Se_3)	633	40815	15.0	468	0.74	−102
Arsenic tritelluride (As_2Te_3)	633	46883	17.28	379	0.60	−38
Germanium disulfide (GeS_2)	1113			765	0.69	−157
Germanium selenide ($GeSe_2$)	1013			695	0.69	−113
Si	1685	50570	7.17			—
ZrF_4	1205	Sublimes at 1177 K		—	—	−1909
BaF_2	1563	28.5	4.35			−1210
NaF	1269	33.5	6.30			−574
ZrF_4-BaF_2 equimolar glass	823			543		
$CdCl_2$	842	30.1	8.55			−392
$BaCl_2$	1195	17.2	2.06			−858
$CdCl_2$-$BaCl_2$ equimolar glass	583			425		

which will aid our understanding of the structure–property relationship. In this process of a comparative analysis of thermodynamic properties, we represent the entropy of melting in Equation 1.2a, which is divided by a factor 4.187, the conversion factor for 1 calorie unit into a joule unit. The ratio in Equation 1.2a, therefore, is redefined in terms of an "entropy unit (eu)" in Equation 1.4 as a measure of disorder:

$$\Delta S_f = \frac{\Delta H^f}{4.187 T_f} (\text{eu}) \qquad (1.4).$$

From this expression, an eu is a measure of disorder at the melting point, which shifts the entropy of a corresponding liquid at T_f along the line BC in Figure 1.1. In Table 1.1, the last but one column gives the ratio T_g over T_f, which is often used to define the glass-forming tendency of a liquid, and is known to vary between 0.60 and 0.80 for most glass formers. We also point out to the reader that the literature frequently uses terminologies such the "glass-forming ability" and "glass-forming tendency" which carry analogous meaning. However, neither of these two terminologies should be confused with the "metastable stability" of a glassy state, which can only be quantified by the kinetics of glass formation. Several glass-stability parameters have also been used in the literature, some of which are explained in the context of the kinetics of glass formation and the classical theory of crystal nucleation and growth.

A comparison of the values of eu for various unary glass formers in Table 1.1 demonstrates that there are unary compounds, namely SiO_2, BeF_2 and GeO_2, which have a relatively lower value of eu (~1.1 to 1.4) on melting, suggesting that the extent of structural disorder as a result of melting at T_f, is comparatively much smaller than any other groups of compounds in this table. The values of eu for arsenic based chalcogenides (As_2S_3, As_2Se_3 and As_2Te_3) are naturally the largest, due to their high vapour pressures at the melting points. Unfortunately, a similar comparison for germanium based chalcogenides cannot be carried out, due to the lack of relevant thermodynamic data in the literature. In Table 1.1 we also find that the values of the ratio of T_g to T_f, for glass-formers such as SiO_2, GeO_2, BeF_2, $ZnCl_2$, S and Se are predominantly in the range 0.65–0.72, which falls in a "*critical undercooling range*" of roughly $^2/_3$ of the corresponding melting point of the unary glass-forming compound. Table 1.1 thus shows two important features: (i) there is an entropic disorder associated with the glass formation in unary compounds and (ii) each glass-former requires undercooling, with respect to melting point. Discussion of the aspects of undercooling and entropic changes associated with glass formation will be resumed later in this chapter and in Chapter 2, to help in explaining the thermal properties and viscosity of various types of glasses.

In Table 1.1 we also compare the lattice energies of commonly known glass-forming compounds and constituent components of multi-constituent glassy phases. The importance of the lattice energies of constituents is explained below in the context of eutectic compositions, at which a vast majority of liquids, when quenched, transform into a glassy phase. The lattice energy of various compounds are best quantified by their heats of formation, which yield the resulting bonds, e.g. in SiO_2 the Si—O bond, as explained by the Born–Haber cycle. In Table 1.1, the values of lattice energies (or the heats of formation) of pure glass-forming elements, namely Si, Se and S, are zero [8]. To estimate the differences in lattice energies of multi-constituent glasses, say, for example, the equimolar compositions for AgI-CsI, the lattice energy difference can be estimated by simply subtracting the value of CsI from that of AgI and dividing it by 2.

A vast majority of practical inorganic glasses used for engineering applications are constituted of more than one component. This means that the thermodynamic properties of liquid mixtures are relevant in the discussion of glass-forming liquids, which may be characterized using the concepts of classical thermodynamics. Comprehensive essays on the properties of liquid mixtures with examples of metallic and inorganic oxides are cited in a number of text books on this subject by the pioneers of applied thermodynamics, Darken and Gurry [10], Swalin [11], Richardson [12], Lupis [13], Turkdogan [9b], and also in classical ceramic and halide salt references [14,15]. The properties of liquid mixtures and the use of phase diagrams for the determination of partial molar quantities of component end members in a binary mixture are especially discussed in References 9b–13. In a binary liquid, for example, in which more than one component is required for glass formation, the overall change in the entropy of a mixture differs significantly. Thermodynamically a binary mixture, for example with X_A and X_B fractions of constituents A and B, respectively, is more stable than the pure constituents, A and B. This becomes apparent when we consider the depression in the melting point of a pure constituent, with respect to a liquidus temperature $(T^l)_i$ at a given mole fraction, X_i, which is analogous to Equation 1.2a:

$$\left(T^{l}\right)_i = \frac{\Delta H^{f} + \overline{\Delta H}_i}{\Delta S^{f} + \overline{\Delta S}_i} \tag{1.5}$$

where $\overline{\Delta H}_i$ and $\overline{\Delta S}_i$ are the partial molar enthalpy and entropy of mixing of a binary mixture. The value of $\overline{\Delta H}_i$ can be assumed to be zero for ideal mixtures. For non-ideal mixtures with negative enthalpy of mixing, the partial enthalpies are also negative in the numerator of Equation 1.5. The denominator, however, has a partial entropy of mixing $\overline{\Delta S}_i$ term, which is always positive, and for a simple ideal mixture it is equal to $-R \ln X_i$. Substituting $-R \ln X_i$ in Equation 1.5 yields Equation 1.6, in which the liquidus temperature, $(T^l)_I$ can be expressed in terms of composition (X_i) and the melting point and entropy of an end member in a binary mixture. Here R is the universal gas constant, with a value 8.314 J mol^{-1} K^{-1} in SI units:

$$\left(T^{l}\right)_i = \frac{\Delta H^{f}}{\Delta S^{f} - R \ln X_i} = \frac{T_f}{\left[1 - \dfrac{R}{\Delta S^{f}}(\ln X_i)\right]} \tag{1.6}$$

From this simple equation we find that for a given value of X_i in a binary or multicomponent liquid the drop in the liquidus temperatures, $(T^l)_I$ is large when the value of ΔS^f is small. In addition, if we consider a non-ideal glass-forming liquid in which the value of $\overline{\Delta H}_i$ is negative, the corresponding reduction in the value of predicted $(T^l)_I$ is expected to be much larger than when a liquid mixture behaves as an ideal mixture. We can, thereby, critically examine examples of glass formation in inorganic glass-forming liquids. Based on such comparisons, the corresponding drop in the liquidus leading to formation of eutectic mixtures is discussed in the context of the partial molar properties of the two binary mixtures. The first glass-forming system is a monovalent mixture of AgI-CsI, followed by the CdF_2-$BaCl_2$ system, and finally a series of tetravalent–monovalent and tetravalent–divalent fluoride liquid mixtures, especially in the ZrF_4-NaF and ZrF_4-BaF_2 systems. These liquids are classed as predominantly "ionic liquids", in which the diffusion of cations and anions is at least 2–3 orders of magnitude larger than in covalent liquids of, say, meta silicates, phosphates and borates. The importance of such a discussion on glass-formation in ionic liquids will become

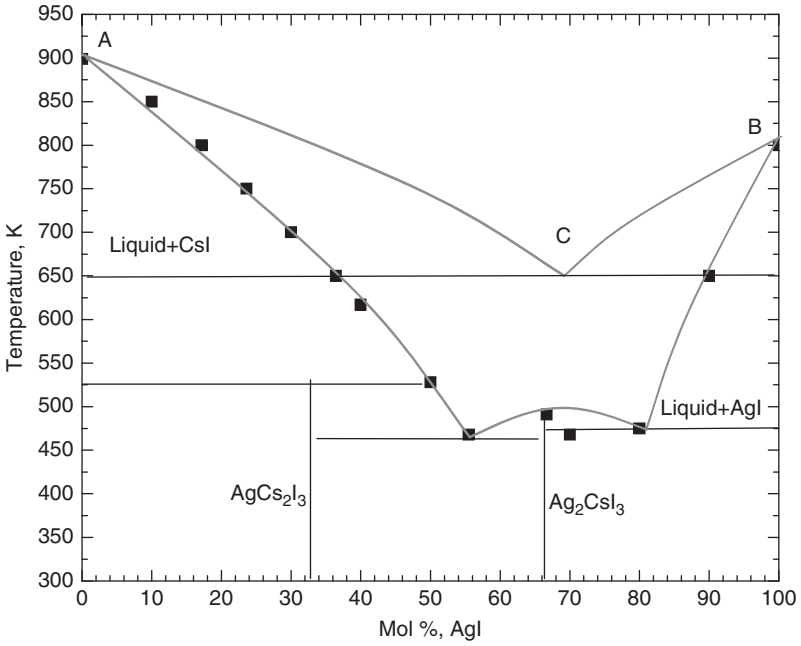

Figure 1.3 *Calculated liquidus lines, AC and BC, are compared with the experimentally determined data [16]. The experimental data also show the presence of complexes, Ag_2CsI_3 and Cs_2AgI_3, and two deeper eutectic temperatures in the vicinity of 450–470 K. Source: Hulme 1989. Adapted with permission from Society of Glass Technology, Sheffield.*

apparent when the tendency for polymerization and evolution of glass-forming networks is discussed by emphasizing the predominance of complex ordering of structures in liquids, as often seen in the properties of silicate, phosphate, germanate, and borate glasses. The nature of such ordering is then manifested through the shape and slopes of liquidus curves in the resulting phase diagrams.

Glass-formation in chloride, bromide and iodide systems, e.g. in the AgI-CsI binary, were first reported by Ding and co-workers [14]. The diffusion coefficient of Ag^+ ions in the AgI-CsI liquids is of the order of 10^{-1} to $10^{-2}\,cm^2\,s^{-1}$ below 100 °C [15]. Hulme and co-workers [16] analysed the phase constitution in AgI-CsI, including the shape of liquidus curve, leading to the formation of eutectic points. The calculated liquidus lines using Equation 1.6 and the empirically determined phase equilibrium boundaries are compared in Figure 1.3, in which it is apparent that the ideal solution model, based on Raoult's law, predicts a eutectic temperature that is ~180 K higher than the actual temperature in the vicinity of 470 K in the binary AgI-CsI system [16]. Evidently, in the AgI-CsI mixture there is a significant departure from ideal behaviour, which can be measured with respect to the value of partial molar enthalpy, $\overline{\Delta H}_i$, in Equation 1.5. A detailed analysis of the partial enthalpy of mixing in the binary halide system may be made using the Hildebrand's Regular solution and Guggenheim models both of which are well cited in the literature.

At the eutectic points the liquid solution freezes and yield solids, as shown in Figure 1.3, two of which are based on silver iodide polyanionic complexes $[Ag_2I_3]^-$ and $[AgI_3]^{2-}$, as shown in Figure 1.4, and form $AgCs_2I_3$ and Ag_2CsI_3 crystals, respectively. As explained by Brink and

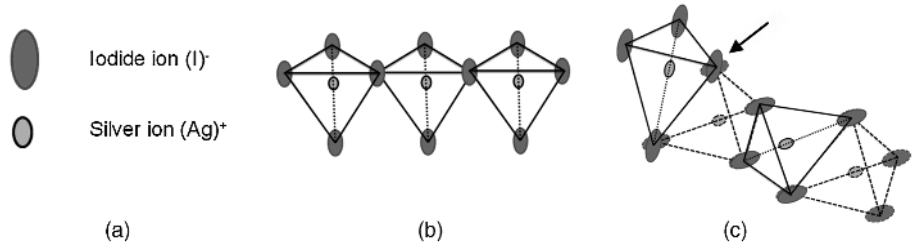

Figure 1.4 *Structures of polyanionic $[MX_3]^{2-}$ and $[M_2X_3]^-$ are shown in (b) and (c), respectively, where (a) large grey and small grey circles represent iodine and silver ions, respectively. (b) Corner shared AgI chains are prevalent in the $AgCs_2I_3$ complex, (c) whereas double edge-shared AgI chains dominate the Ag_2CsI_3 structures. The dotted pyramids in (c) represent the backplane of the paper, which is why along a shared edge four-iodine ions are shown, (see arrow) and is not required in the building of this structure. At other shared edges in (c) this is not apparent [16–18]. Source: Hulme 1989. Reproduced with permission from The Society of Glass Technology, Sheffield.*

co-workers [17], the $[M_2X_3]^-$ and $[MX_3]^{2-}$ form via edge-sharing and corner-sharing, which has been further explained by Wells [18] in his treatise on structural chemistry. The cationic radii of Ag^+ and Cs^+ are 0.127 and 0.168 nm, respectively, and the corresponding values of electronegativity are 1.9 and 0.7, which imply that in the $[M_2X_3]^-$ and $[MX_3]^{2-}$ complexes the Ag^+ cations, due to their smaller size and larger electronegativity than the Cs^+ ions, are responsible for the formation of $[M_2X_3]^-$ and $[MX_3]^2$ polyanionic species (Figure 1.4).

The second example of polymerization in ionic liquids is illustrated by the examples of glass formation in CdF_2-$BaCl_2$, which was reported by Poulain and Matecki [19]. An essential aspect of structural analysis in the divalent mixture is the Gibbs energy of mixing, which is a means of identifying how far a glass-forming solution departs from an ideal Raoult's law, as explained above in Equations 1.5 and 1.6. The determination of non-ideality in CdF_2-$BaCl_2$ can be explained by introducing a thermodynamic term, which will help later on in establishing the relationship between the viscosity and glass structure, IR absorption and spectroscopic properties.

The departure from non-ideal Raoult behaviour of a reciprocal salt mixture, CdF_2-$BaCl_2$, can be defined by calculating the entropy of mixture. When a solid mixture of CdF_2-$BaCl_2$ is heated above the melting points of it constituents, the following ionic exchange reaction occurs:

$$CdF_2(l) + BaCl_2(l) = CdCl_2(l) + BaF_2(l) \tag{1.7a}$$

$$\Delta G_{1.7a} = -38650 - 18.3T \text{ J mol}^{-1} \tag{1.7b}$$

In Equation 1.7a we observe that as a result of ionic exchange $CdCl_2$ and BaF_2 are produced. However, if the solution were an ideal one, the difference in the entropies of unmixed solid states before melting (S_{unmix}) and after melting (S_{mix}), $\Delta S_{\text{mixture}}$, is equal to zero. This means that there is no preferential structural association by forming a polyanionic complex in liquids. In reality such ideal behaviour is much rarer than the non-ideal, and as a result of mixing in CdF_2 and $BaCl_2$, the large difference in their lattice energies (enthalpy of compound formation), the heat or enthalpy of mixing is not zero (see Equation 1.6). This means that in Equation 1.5 the partial thermodynamic quantities in the numerator and denominator become non-zero, and consequently the preferential structural association for complex formation is likely to increase. Thus the "ideal configurational entropy", which can be

expressed by $-R \ln X_i$ in Equation 1.6, is no longer sufficient but will require an additional component, called the thermal component (S_{th}). The thermal component of entropy of a salt mixture was introduced by Richardson [12b]; for reciprocal salt mixtures, the change in thermal entropy (ΔS_{th}) is expressed in terms of enthalpy change (ΔH) in Reaction 1.7a and is equal to equilibrium constant ($K_{1.7a}$):

$$K_{1.7a} = \exp\left[-\frac{\Delta G_{th}}{RT}\right] = \exp\left[-\frac{\Delta H\left(1-\frac{T}{12500}\right)}{ZRT}\right] \quad (1.8).$$

Here Z, R and T are the cation co-ordination number in the polyanion structure, universal gas constant and absolute temperature, respectively. Richardson explained that the thermal contribution to entropy of a reciprocal mixture can be estimated by the change in the lattice energies or enthalpy (ΔH) and is equal to (ΔH)/12500, which is shown in Equation 1.8. The Gibbs energy change (ΔG_{th}) for reaction, given in Equation 1.7b [20], yields a value of (ΔS_{th}) of −3.07, suggesting that the overall change in the entropy should shift towards a more preferential association for a $CdCl_2$-BaF_2 distribution than a CdF_2-$BaCl_2$ type association. From Equation 1.8 the non-ideality yields a value of $K_{1.7}$ equal to 1.735 at 973 K, which from Equation 1.7b yields a value of 36.75% for the preponderance of $CdCl_2$-BaF_2. This value of preponderance is measured with respect to an ideal state having random association. Therefore, based on the differences in the lattice energies of $BaCl_2$, BaF_2, CdF_2 and $CdCl_2$, the following polyanionic species are likely to make the 36.75% excess of preferential association for Cd—Cl bonds, compared to Cd—F bonds as shown in reactions 1.9a to 1.9c:

$$CdCl_2(l) + BaCl_2(l) = [CdCl_4]^{2-}(l) + Ba^{2+}(l) \quad (1.9a)$$

$$CdCl_2(l) + BaF_2(l) = \left[Cd(Cl_{0.5}, F_{0.5})_4\right]^{2-}(l) + Ba^{2+}(l) \quad (1.9b)$$

$$CdF_2(l) + BaF_2(l) = [CdF_4]^{2-}(l) + Ba^{2+}(l) \quad (1.9c)$$

$$CdCl_2(l) + KCl(l) = [CdCl_3]^{1-}(\ell) + K^{1+}(l) \quad (1.9d)$$

The polyanionic species $[CdCl_4]^{2-}$ is analogous in chemical character to $[ZnCl_4]^{2-}$ in $ZnCl_2$-based glass-forming liquids. Matecki and Poulain [19] also reported that in the CdF_2-$BaCl_2$ glass forming liquid the incorporation of alkali fluorides and chlorides aids the glass formation. The presence of KCl, for example, promotes formation of $[CdCl_3]^-$ via the reaction shown in Equation 1.9d.

So far, it is apparent from the thermodynamic analysis that the reciprocal salt mixtures, namely $CdCl_2$-BaF_2, promote glass formation due to the presence of polyanionic species, such as $(CdCl_4)^{2-}$ and $(CdCl_3)^-$, which are stabilized in the presence of cations with a large coordination field ($z = 8$), e.g. Ba^{2+} and K^+. The preponderance of polyanions arises due to a large difference in the lattice energies of constituents of a glass-forming liquid.

The final example of the dominance of polyanionic species near glass-forming compositions is taken from the ZrF_4-BaF_2-NaF system, in which the lattice energies of ZrF_4, BaF_2 and NaF are vastly different from each other, since none of the two fluorides have comparable crystal structures. The barium fluorozirconate liquids, when mixed with NaF, form a range of glasses that were first reported by Poulain and co-workers [21]. The thermodynamic properties of barium fluorozirconate and sodium fluorozirconate liquids were analysed by Grande and

co-workers [22,23] and Hatem and co-workers [24]. Grande *et al.* adopted the non-ideal solution model for determining the molar heats of mixing for ZrF_4-NaF and ZrF_4-BaF_2, showing the minima at around 40 mol.% ZrF_4, where the glass-forming tendency is maximized. The corresponding binary diagrams can be seen in Figure 1.5a and b, respectively.

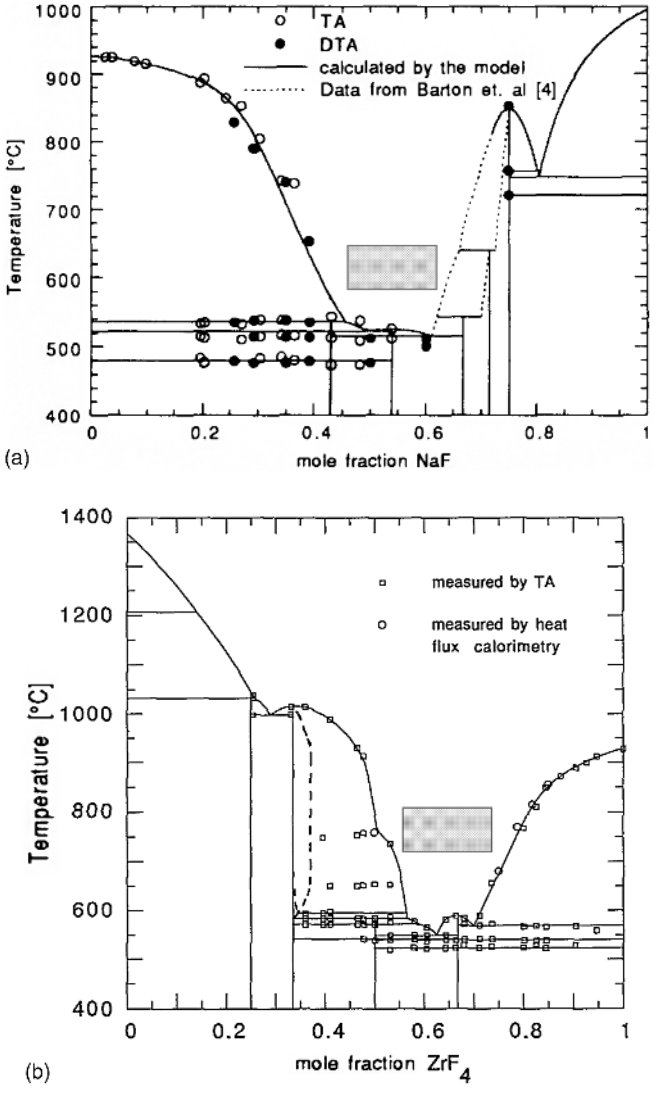

Figure 1.5 *(a) Phase-equilibrium boundaries in the NaF-ZrF_4 system, determined by Grande and co-workers by using the experimental data and a thermodynamic model [22,23]. The shaded area near equimolar NaF:ZrF_4 shows the regions of glass formation, when mixed with BaF_2. Adapted from the original in References 22,23. (b) Comparison of the experimentally determined phase-equilibrium boundaries in the BaF_2-ZrF_4 system, determined by Grande and co-workers [22,23]. The shaded area near equimolar BaF_2:ZrF_4 is the composition range of enhanced glass formation, when mixed with NaF. Adapted from the original in References 22 and 23. Source: T. Grande 1992. Reproduced with permission from Elsevier limited.*

Two major reviews by Poulain [25] and Parker [26] have explained that the ZrF_4-BaF_2 is a conditional glass former, and the incorporation of a third constituent, namely NaF or AlF_3, enhances the glass formation tendency by increasing the Coulombic asymmetry or the asymmetry in the lattice energies. The magnitude of asymmetry in the lattice energy of constituents, resulting in the formation of a non-ideal glass-forming liquid in ZrF_4-NaF-BaF_2, was characterized by Grande and co-workers [21,22] by plotting the enthalpy of mixing energies of the binary constituents and the dominance of the complex fluorides in the intermediate composition range in the ZrF_4-BaF_2-NaF (Figure 1.6a and b). Such profound experimental evidence reinforces the point made earlier in this section with reference to Equation 1.5 that the tendency for complex or compound formation in a binary and ternary phase diagram lowers the melting point (cf. Equation 1.5), as also shown in Figures 1.3, Figures 1.5a and 1.5b, and therefore promotes the glass formation.

From the examples above on molten salts, it is apparent that a strong tendency for complex formation in binary and pseudo-binary phase diagrams coincides with the glass-forming compositions. The glass-forming liquids are strongly non-ideal solutions, as depicted by the dominance of complex formation in examples of AgI-CsI, $CdCl_2$ and ZrF_4 based compositions, e.g. in Figure 1.6b. Finally, as the magnitude of Coulombic charge difference among

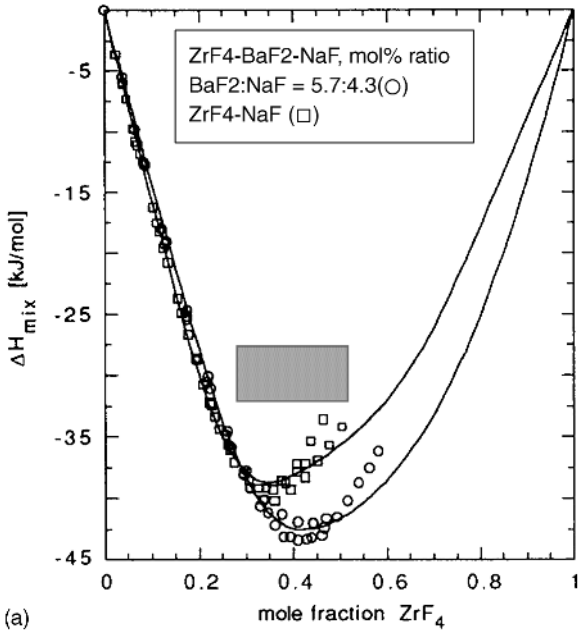

Figure 1.6 *(a) Asymmetric parabolic shape of heat of mixing (ΔH_{mix}, kJ mol^{-1}) for the ZrF_4-BaF_2-NaF and ZrF_4-NaF mixtures are plotted against the mole fraction (X_i) of ZrF_4 as a constituent of the mixture. The position of the minimum designates the likelihood of formation of complexes, which are shown (b) [22,23] and coincides with the stable glass-forming range, designated by the shaded area. Source: T Grande 1993. Reproduced with permission from Elsevier limited. (b) Plot of the number of moles of complexes, as an example, which form in the binary ZrF_4-NaF mixture, as a function of the mole fraction (X_i) of ZrF_4 which is based on the thermodynamic model for solutions [22]. Source: T Grande 1993. Reproduced with permission from Elsevier.*

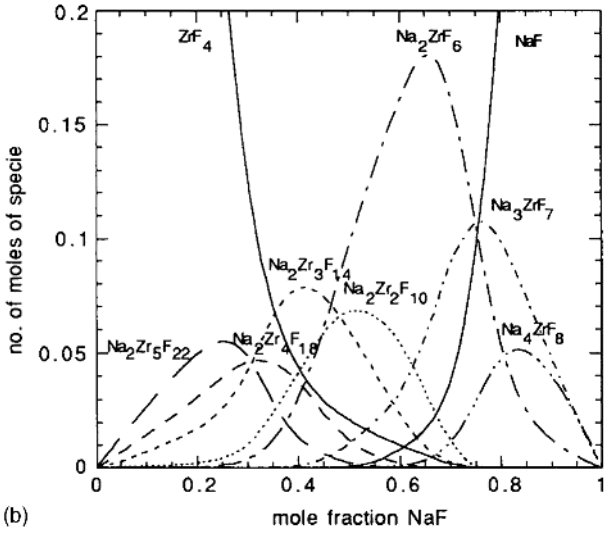

Figure 1.6 *(Continued)*

the cations involved in defining a glass-forming composition increases, the magnitude of partial molar quantities also tends to depart further from the idealized behaviour.

Having analysed the thermodynamic properties of glass-forming liquids in binary and pseudo-binary phase diagrams, it is possible to draw general conclusions that for complex polyanions to exist a central cation charge (e.g. Ag^{+}, Cd^{2+}, Zr^{4+}) needs a strong polyhedron cage, to support the structure through bonding with large anions (F^{-}, Cl^{-}, and I^{-}). The experimental proofs for such a polyanionic structure in glass-forming liquids appears to have a similarity with Zachariasen's random network model for covalent glasses and Goldschmidt's cation-to-anion ratio. In AgI-CsI, the complexes $[AgI_3]^{2-}$ and $[Ag_2I_3]^{-}$ tetrahedra and polyhedral structures may be compared as the building blocks with the random polyanion networks of $[SiO_4]^{4-}$, $[PO_4]^{3-}$ etc. in a covalent glass. The polyanions of $(Cd\{FCl\}_4)^{2-}$ in CdF_2-$BaCl_2$ and $[ZrF_6]^{2-}$ in ZrF_4-BaF_2-NaF glass-forming systems are essential for supporting the three-dimensional random networks.

For the analysis of structures in inorganic glasses, the cationic radii (R_C in nm) and Pauling's electronegativity for a cation–anion pair ($\Psi_{C\text{-}A}$), average co-ordination number (Z_c), and their effect on lattice energy (ΔH_{lat}) for representative glass-forming compounds are discussed.

1.5 Glass Formation and Co-ordination Number of Cations

Before discussing the details of glass structure, it is essential that we introduce the concept of electronegativity and co-ordination number of cations for several inorganic glass-forming compounds. The electronegativity is the tendency of an atom to attract another electron to complete a pair state of electrons in the outermost orbit of the valence band. In the periodic table, the elements are more electropositive on the left-hand side than the elements on the

right-hand side, e.g. the group VII halogen elements, namely F, Cl, Br and I, which are electronegative. The elements in the middle of periodic table are neither strongly electropositive nor electronegative, and therefore tend to form bonds with both types of elements. This tendency for combining with another element determines the residual electronegativity of a bond, which in turn determines the magnitude of enthalpy of mixing in a complex glass-forming liquid. From Equation 1.5, therefore, a change in the slope of liquidus curve will be expected, depending upon the magnitude of the partial molar enthalpy of a mixture.

Among the structural models for glass formation, the Zachariasen rules [27] is the first one considered here. The original rule has been strictly developed for covalent oxide glass-formers which depict a three-dimensional continuous network of cation–anion pairs of bonds. This rule adapted the solid-state chemical structural evidence of crystalline materials to postulate the structural chemistry of covalently bonded glass networks. The interatomic forces are comparably similar in a glass and its parent crystal, which then implies naturally that the chemical bonds and the nearest neighbour cation–anion co-ordination in glass and crystals are likely to be similar. Since a glass is derived by quenching a liquid it must be at a higher energy state than the corresponding equilibrium solid, as depicted in Figure 1.1.

By defining the above postulations, Zachariasen specifically defined the model for silica glass which was subsequently found to be consistent with the X-ray diffraction data of Mozzi and Warren [28]. From the Zachariasen model applied to silica, each Si^{4+} cation must be connected to at least one O^{2-}, if not more, resulting in an average co-ordination of between 3 and 4, based on the $[SiO_4]^{4-}$ crystal model where each silicon (Si^{4+}) is surrounded by four oxygen (O^{2-}). The resulting tetrahedron must share at least one corner with a neighbour with the maximum number of shared corners being four. According to this rule, the edge and face sharing of polyhedron may not be possible. The co-ordination with a neighbouring polyhedron may be continuous, yielding a three-dimensional continuous random network. The continuous network model then further specifies the nature of oxygen as the bridging oxygen atoms between two silicons (≡Si—O—Si≡) and the non-bridging oxygen atoms (≡Si—) in which one of the oxygen sites is unoccupied. In this representation the ≡ symbol represents three other oxygen-bridged sites around silicon. In view of the covalent nature of groups IVB (Si, Ge), VB (P) and III (B), the Zachariasen model seems to work reasonably well and has been found to be consistent with the large number of experimental data on silica, silicates, phosphates, germanium oxides and borate glasses. However, for large cationic co-ordination system the rules seem to break down.

Pauling's electronegativity for a cation (C) and anion (A) pair ($\Psi_{C\text{-}A}$) is given by Equation 1.10 in which the unit of dissociation energies, E_d, of the A—C, A—A and C—C bonds are in electron volts; a factor $(eV)^{-0.5}$ is then included for a dimensionless $\Psi_{C\text{-}A}$: [29]

$$\psi_{C-A} = \left(\sqrt{(E_{C-A}) - \left[\frac{E_{AA} + E_{CC}}{2} \right]} \right) x(eV)^{-0.5} \tag{1.10}$$

Based on Pauling's model in Equation 1.10, the difference in Pauling's electronegativity between silicon and oxygen is 2.59, which is derived from the value of enthalpy of formation of SiO_2 at 298 K as a reference state. Since the enthalpy of formation, which corresponds to the Si—O bond, is 9.40 eV the value of ($\Psi_{C\text{-}A}$) can be derived, using the electronegativity data for oxygen and Si, which are 3.44 and 1.90 eV, respectively from the *Wikipedia* reference [29] above in Equation 1.10. For such comparisons it is easier to consider the readily available

Table 1.2 *Comparison of Pauling's electronegativity data with the entropy of fusion (ΔS^f, eu) for several glass-forming compounds for which cationic co-ordinations are also included. Py: pyramid, Ch: chain, BPy: bipyramid, Tr: tetrahedron, Oct: octahedron, C: cube.*

Compounds	Z_c	$\Psi_{C\text{-}A}$	R (Å)	ΔS_f, (eu)	Structure	R_C/R_A	Remarks
B_2O_3	3, 4	3.16, 1.68	1.55	7.33	Py, Tr	0.17	
As_2O_3	2, 3	1.11		7.2	Ch, Tr	0.43	Sublimes
SiO_2	4	2.59	1.74	1.08–1.30	Tr	0.31	
BeF_2	4	2.39	1.68	1.37	Tr	0.26	
GeO_2	4, 6	1.8, 1.08	1.85	1.4	Tr, Oct	0.40	
P_2O_5	4	3.68	1.67	13.6	Tr	0.26	Sublimes
V_2O_5	4	3.53	1.91	16.54	Tr	0.44	sublimes
GeS_2	4	0.81	2.37	5.74?	Tr	0.29	
$ZnCl_2$	4	1.32	2.55	4.14	Tr	0.41	
TeO_2	4, 6	0.76	2.02	6.91	BPy, PyPy	0.53, 0.42	
WO_3	4	2.39	1.94	10.06			
Al_2O_3	4–6	3.87	1.83	11.06	Oct, BPy, Tr	0.38	
Bi_2O_3	6	1.373	2.28	13.03	Oct	0.72	
Ga_2S_3	4, 6	2.29	2.46	?	Oct, Tr	0.33	Data unknown
ZrF_4	6	4.15	2.12	?	Oct	0.59	Sublimes
La_2O_3	6	4.03	2.71	?	Oct, 7- & C	0.77	Data unknown
La_2S_3	6	3.49	3.23	?	Oct, 7- and C	0.55	Data unknown
S	2	2.58	1.84	1.02	Ch		
Se	2	2.55	1.91	2.84			
As_2S_3	4	−0.8	2.42	11.7	Ch,	0.25	
AgI	4	−1.286	3.46	2.7	Tr	0.57	
CsI	8	1.32	3.87	6.4	C	0.76	

data for the enthalpy of formation of a compound at 298K than to hunt for the bond-pair energy which is not listed for the complex glass-forming compounds. In Table 1.2, the computed values of ($\Psi_{C\text{-}A}$) for glass-forming compounds are compared with ΔS^f, discussed above in Table 1.1. The data in Table 1.2 are also compared with the average co-ordination number of cations in the crystalline state. The bond lengths (R, Å) in Table 1.2 are represented by the sum of cationic and anionic radii, assuming that each cationic sphere is in physical contact with Z anionic spheres. The data in Table 1.2 have been plotted to show a trend in glass-forming behaviour in Figure 1.7. In Figure 1.7 the values of ($\Psi_{C\text{-}A}$), representing the bond pair of network forming compounds, are plotted against their entropy of fusion, ΔS^f.

For example, the values of electronegativity for glass-forming compounds with $Z = 4$, namely, SiO_2, BeF_2, GeO_2, $ZnCl_2$ and TeO_2, exhibit a trend in which the electronegativity of glass-forming compounds decreases with increasing entropy of fusion (in eu). This trend in Figure 1.7 also implies, from Equation 1.6, that the depth of a eutectic point with respect to the melting point increases when constituting liquidus regions are in equilibrium with solids having such low values of entropy of compounds. The deep eutectic condition favours the formation of glass on quenching such liquids. Other glass-forming materials, such as S and Se, also follow this dependence on the entropy of fusion. However, for all other Z values except $Z = 2$ and 4, the relationship shown in Figure 1.7 does not apply universally, due to the absence of the known glass-forming systems, e.g. in the family of $Z = 3$, 5 and 6. Especially

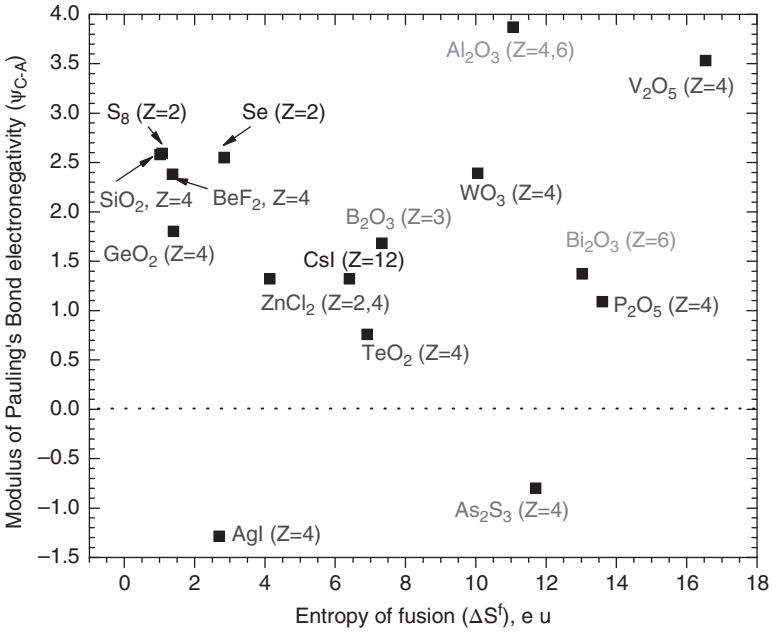

Figure 1.7 *Plot of Pauling's bond electronegativity ($\Psi_{C\text{-}A}$) against entropy of fusion (ΔS^f) of the glass-forming compounds listed in Table 1.2.*

for $Z = 6$ there is no apparent relationship between Al_2O_3, Bi_2O_3, and vanadate, niobate and tantalite family of glass forming networks. In addition, B_2O_3 cannot be compared with any other compound with $Z = 3$ in this figure, because it is neither isochemical nor isostructural with other glass-forming compounds in Figure 1.7. By contrast, we also find that the value for As_2O_3 differs from P_2O_5. Note also that the values of $(\Psi_{C\text{-}A})^2$ for As_2S_3 and AgI are negative because the enthalpy of formation, which yields the value of first term within the square root equation in Equation 1.10, is too small and as a result the whole term within the root becomes negative, which mathematically has little meaning in the context of electronegativity. Compounds such as WO_3, V_2O_5 and Al_2O_3 are conditional glass-formers, as is TeO_2, and each require another compound to be present in the liquid for glass formation.

Figure 1.7 is a plot of two structure sensitive properties ($\Psi_{C\text{-}A}$) for the analysis of strong, intermediate and weak tendencies for glass formation, which we may also be amenable to comparison with Sun's single bond [30] and Rawson's bond-strength-freezing point [31] models. The details of the Rawson's models have been discussed in detail by Varsheneya [3b], which may be useful supplementary reading on the bond energy data for glass forming, intermediates and modifier oxides. By comparison, the E_b (kJ mol^{-1}) values fall into three different types of oxides playing a different role in the glass formation. According to Sun's model glass-forming compounds (B_2O_3, SiO_2, GeO_2, P_2O_5, and BeF_2) have E_b values larger than ~360 kJ mol^{-1}. By comparison the modifying oxides (Na_2O, K_2O and CaO) have E_b values lower than ~220 kJ mol^{-1}. Between the two extreme limits of glass-formers and modifiers fall the E_b values of intermediate compounds. Unlike the rigorous thermodynamic approach discussed above, neither Sun's model nor the electronegativity model is able to explain the negative values of $(\Psi_{C\text{-}A})^2$ for As_2S_3 and AgI (Figure 1.7). As will be explained in subsequent

chapters, a rigorous approach based on thermodynamic and kinetic models is the best approach in the analysis of glass-formation that must be adopted for engineering of a glass composition and its stability.

Many of the compounds in Table 1.2 manifest multiple co-ordination numbers, especially when they are present in a glassy matrix in which the three-dimensional lattice constrains are significantly reduced. Classical examples of multiple co-ordination shells are in tetrahedron co-ordination (fourfold) in $[AlO_4]^{5-}$, bipyramid (fivefold) co-ordination in $[AlO_5]^{4-}$, and octahedron (sixfold) co-ordination in $[AlO_3]^{3-}$, as well as prismatic B in $(BO_3)^{3-}$, tetrahedral co-ordination in $(BO_4)^{5-}$, bipyramid Te in $(TeO_4)^{4-}$, prismatic Te in $(TeO_3)^{2-}$ and polyhedron Te in $TeO_{3+\delta}$. Since the co-ordination shell structures determine the band gap energy, any change therein is likely to influence the UV-visible and vibrational spectroscopic, thermal and viscosity properties of a glass. The argument for co-ordination polyhedra in glass-forming systems is consistent with the Zachariasen model which is based on the parent crystalline solid, in which cation and anion pair is comparable with that of crystalline solids. Amongst various oxides, Al^{3+} as a cation has a complex co-ordination shell that is observed in both the oxide and fluoride glasses, in which the ion may be present as network former, intermediate and modifier in a composition range. Simmons and co-authors [32] have explained in detail the importance of co-ordination polyhedra for cations in the context of fluoride glass structure in which the authors have used the cation-to-anion radius (R_c/R_A) ratio as a good approximation for the description of a co-ordination polyhedron. For this reason, the Ag^+ ion in Figure 1.4 is surrounded by four iodine ions in tetrahedron symmetry because of the size difference, which is pointed out in Table 1.2.

Recently several methods for quantifying the ionicity of a bond pair have been reported using both the empirical [33] and theoretical approaches, including first principle [34] and density functional theory [35], for many ionic and semiconductor compounds. Based on reasonable comparison of data between the empirical [33] and theoretical [34,35] approaches, Al-Douri compared the data for a range of semiconductors and found reasonable agreement between his computed data and that reported by Phillips [36]. This method may be found useful for chalcogenide glasses, based on the elements belonging to groups IV, III–V, and II–VI. Furthermore, the ionicity model for chalcogenides may also be supplemented by the estimation of co-ordination number using the Mott's 8–N (also known as the octet) rule and Phillip's "bond-stretching and bond-bending" model. The latter appears to be specifically relevant in the context of glass formation in Ge-Se system.

Besides Pauling's electronegativity discussed above, another model was proposed by Sanderson, which adopts a different representation by considering the molecular bond electronegativity as a geometric mean of a formula unit, C_mA_n, where C and A, as explained above, designate a cation and an anion, respectively [37]. The geometrical mean of the Sanderson electronegativity $(\psi_{C\text{-}A})^S$ then equals:

$$(\psi_{C-A})^S = \sqrt[m+n]{(\psi_C)^m \cdot (\psi_A)^n} \tag{1.11}$$

which for alumina (Al_2O_3), $(\psi_{C\text{-}A})^S$, is equal to:

$$(\psi_{Al-}O)^S = \sqrt[5]{(\psi_{Al})^2 \cdot (\psi_O)^3} = \sqrt[5]{(2.22)^2 \cdot (5.21)^3} = 3.703$$

compared to 3.87 computed from Equation 1.10 in Table 1.2 using Pauling's model. Values of Sanderson electronegativity have been compiled by West [37], where the values of partial charge on oxygen for a cation–anion pair ($-\delta_O$) are also reported. Note that the partial charge

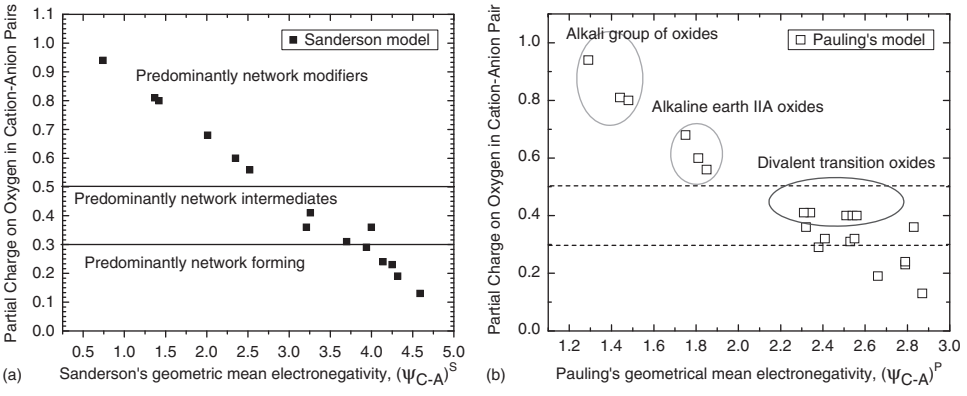

Figure 1.8 *(a) Plot of partial charge on oxygen in cation–anion bonds against the values of Sanderson electronegativity $(\psi_{C\text{-}A})^S$. (b) Pauling's geometric mean values plotted against the partial charge on oxygen on cation–anion pairs.*

on an anion is a negative quantity. By plotting the values of partial charge on oxygen in cation–anion pairs in oxides in Table 1.2 against the values of Sanderson electronegativity, a reasonable trend between the glass network formers, contributors and modifiers is observed (Figure 1.8a), and is characteristically absent in Figure 1.7. The corresponding data for various oxides used in Figures 1.8a and 1.8b are shown in Table 1.3, from which the

Table 1.3 *Partial charge on anions $(-\delta_A)$ for oxides and chlorides [37]. Source: A. R. West 1988. Reproduced with permission from John Wiley & Sons.*

Compounds **Monovalent**	$(-\delta_O)$	Compounds **Divalent**	$(-\delta_O)$	Compounds **Trivalent**	$(-\delta_O)$	Compounds **Tetravalent**	$(-\delta_O)$
Cu_2O	0.41	HgO	0.27	Ga_2O_3	0.19	CO_2	0.11
Ag_2O	0.41	ZnO	0.29	Tl_2O_3	0.21	GeO_2	0.13
Li_2O	0.8	CdO	0.32	In_2O_3	0.23	SnO_2	0.17
Na_2O	0.81	CuO	0.32	B_2O_3	0.24	PbO_2	0.18
K_2O	0.89	PbO	0.36	Al_2O_3	0.31	SiO_2	0.23
Rb_2O	0.92	SnO	0.37	Fe_2O_3	0.33	MnO_2	0.29
Cs_2O	0.94	FeO	0.40	Cr_2O_3	0.37	TiO_2	0.39
		CoO	0.40	Sc_2O_3	0.47	ZrO_2	0.44
		NiO	0.40	Y_2O_3	0.52	HfO_2	0.45
		MnO	0.41	La_2O_3	0.56		
		BeO	0.36				
		MgO	0.50				
		CaO	0.56				
		SrO	0.60				
		BaO	0.68				
Chloride compounds							
CuCl	0.29	RbCl	0.78	$CdCl_2$	0.21	$BaCl_2$	0.49
AgCl	0.30	CsCl	0.81	$BeCl_2$	0.28		
LiCl	0.65			$MgCl_2$	0.34		
NaCl	0.67			$CaCl_2$	0.40		
KCl	0.76			$SrCl_2$	0.43		

chemical character of glass network formers, contributors or intermediates and modifiers may be identified.The graphical relationships shown in Figures 1.8a and 1.8b are similar, except that in Figure 1.8b we have also included the data for divalent transition metal oxides (MnO, FeO, NiO, CoO and CuO) and for BeO, MgO and ZnO. All five divalent transition metals fall between network intermediates and divalent alkaline earth oxides.

In figure 1.8a, the network glass-formers are at the bottom right-hand corner, above which the network contributors cluster together with the transition metal oxides. The network modifiers of alkali and alkaline earth oxides lie at and above a partial charge on oxide of 0.5.

Continuing with the partial charge on the anion (e.g. oxygen for oxides), on comparing the values of partial charge on oxygen on different types of oxides in Table 1.3 with the values of entropy of fusion for oxides in Table 1.2 it is qualitatively apparent that the entropy of fusion scales with the partial charge on oxygen and with Pauling's and Sanderson's electronegativity. The glass-forming network compounds have smaller values of δ_O and entropy of fusion, in general. This trend seems to apply satisfactorily to all glass-forming networks for which the values of δ_O are known, which helps in understanding the chemical character of various compounds that partake in the constitution of a glass.

Table 1.3 also includes data for chlorides, for which a comparable trend amongst network formers, contributors and modifiers is apparent, especially when comparing the residual charge on chloride ions in $BeCl_2$ and $CdCl_2$.

A summary of the analysis of electronegativity therefore clearly demonstrates that it is the residual charge ($-\delta_A$) on anions in a compound that may be responsible for determining the structural role in glass-forming liquids and glasses. There is also a qualitative relationship between the entropy of fusion, δ_A, and $\psi_{C\text{-}A}$ (Pauling and Sanderson). Based on the concepts of electronegativity, we now introduce the ionicity of a bond and discuss it in the context of a glass network.

1.6 Ionicity of Bonds of Oxide Constituents in Glass-Forming Systems

There are several models used in the calculations of ionicity of atoms, simple and complex bond pairs. This is especially relevant in the analysis of the ionic character of bond termination sites, which may be at the surface and in the bulk. For bond termination sites, which are known as the non-bridging sites, the analysis of ionicity is important for determining not only the energetics of the cation environment but also its likely co-ordination field. In other words the ionicity is an important factor that is essential in the characterization of cationic co-ordination in crystals and glass hosts.

By considering the lattice energy and electronegativity models, proposed by Liu and co-workers [38] and Zhuralev [39], respectively it is possible to explain the two main contributing factors of a bond, namely, the ionic (U_{ion}) and covalent ($U_{covalent}$) parts of the lattice energy, as shown in Equation 1.12:

$$U_{total} = U_{ion} + U_{covalent} \tag{1.12}$$

Considering the bonding in crystals as a first approximation of a corresponding glassy structure, we may be able to use the Kapustinskii equation [40] shown in Equation 1.13, to describe the ionic part of the total lattice energy. We also assume that not all the bonds are

alike in complex crystals:

$$U_{\text{ion}}\left(\text{kJ mol}^{-1}\right) = \left[\frac{1270(m+n)Z_C Z_A}{d}\right]\left(1 - \frac{0.4}{d}\right)f_i \tag{1.13a}$$

$$U_{\text{covalent}}\left(\text{kJ mol}^{-1}\right) = \left[\frac{2100m(Z_C)^{1.64}}{d^{0.75}}\right]f_i \tag{1.13b}$$

Here d is the bond length, Z_A and Z_C are the valencies of cations and anions, respectively, and m and n are the corresponding stoichiometric indexes in the compound A_mO_n. From these two equations and the values of average band gap energy (E_g), which is composed of homopolar (E_{homo}) and heteropolar (E_{hetero}) parts of the overall bonding, such that the $\left(E_g\right)^2 = (E_{\text{homo}})^2 + (E_{\text{hetero}})^2$ [41]. Based on the approach discussed above, the derived values of ionicity of bonds are summarized in Table 1.4.

Zhuralev on the other hand, using the electronegativity model, has given the calculated values of ionicity of elements with varying co-ordination number for the cation–oxygen bridge. Table 1.5 shows the values of ionicity for MO_6 and AO_4 co-ordination polyhedron. The values for $L = 1.5$ co-ordination in MO_6 and $L = 1.4$ co-ordination in AO_4 are compared

Table 1.4 *Bond lengths (*d *in Å), bond Ionicity (*fi*), and calculated values of* $U_{covalent}$, U_{ionic}, *and* U_{Total} *(all in kJ mol*$^{-1}$*) of some simple crystals with only one type of bond. The values of* f_i *are taken from Reference [39]. Source: V. D. Zhuralev 2007. Reproduced with permission from Springer.*

Crystals	d	f_i	f_i (*Experiment*)	U_{covalent}	U_{ionic}	U_{Total}	$U_{\text{reference}}$	$U_{\text{experimental}}$
LiF	2.01	0.914		107	925.2	1032	1028	1036
NaCl	2.82	0.936		62	723	785	805	786
KI	3.53	0.948		42	605	647	656	649
RbCl	3.29	0.956		38	648	686	690	689
CsBr	3.62	0.965		28	602	630	625	631
CuCl	2.34	0.882		131	794	925	921	996
$SrCl_2$	2.99	0.968		92	2137	2229	2127	2156
MgF_2	1.992	0.911		347	2785	3132	2913	2957
CaO	2.405	0.916	0.74 ± 0.26	295	3215	3510	3414	3401
MnO	2.22	0.887		406	3325	3731	3724	3745
CoO	2.13	0.858	0.70	527	3324	3851	3837	3910
BaO			0.76 ± 0.23					
MgO			0.66 ± 0.16					
ZnO			0.60 []					
GeO_2	1.88	0.730		3430	9317	12748	12828	
SnO_2	2.054	0.784		2735	9201	11936	11807	
SiO_2			0.25					
LaN	2.65	0.759		1477	5559	7036	6876	6793
NbN	2.35	0.720		1877	5812	7689	7939	8022
SrS	3.01	0.917		238	2684	2922	3006	2848
BeS	2.105	0.611		1457	2389	3846	3927	3910
MgTe	2.77	0.589		1253	1848	3101	2878	3081
BaTe	3.179	0.897		283	2506	2789	2721	2843

Table 1.5 *Ionicity values for elements in MO_6 and AO_4 polyhedral units with co-ordination L = 1.5, and L = 1.4, respectively.*

M	Ionicity (δ) for MO_6 co-ordination polyhedral where the magnitude of L designates the number of M—O bridges				
	$L=1$	$L=2$	$L=3$	$L=4$	$L=5$
Li	0.84	0.84	0.84	0.84	0.83
Na	0.85	0.85	0.84	0.84	0.84
K	0.86	0.86	0.86	0.85	0.85
Cs	0.87	0.87	0.87	0.86	0.86
Cu	0.79	0.78	0.78	0.78	0.77
Be	0.7	0.69	0.69	0.68	0.67
Mg	0.73	0.73	0.72	0.72	0.71
Ca	0.75	0.74	0.74	0.74	0.73
Sr	0.75	0.75	0.74	0.74	0.73
Zn	0.7	0.69	0.69	0.68	0.67
Cd	0.7	0.7	0.69	0.68	0.67
Pb	0.74	0.74	0.73	0.72	0.71
Ni	0.74	0.73	0.72	0.71	0.7
B	0.62	0.61	0.59	0.57	0.54
Al	0.68	0.67	0.66	0.64	0.62
Ga	0.65	0.64	0.63	0.61	0.59
In	0.68	0.67	0.66	0.64	0.62
Tl	0.67	0.65	0.64	0.62	0.6
Sc	0.68	0.68	0.66	0.65	0.63
La	0.7	0.69	0.68	0.67	0.65
Bi	0.67	0.66	0.65	0.63	0.61
Mn	0.66	0.65	0.64	0.62	0.6

	$L=1$	$L=2$	$L=3$	$L=4$		$L=1$	$L=2$	$L=3$		$L=1$	$L=2$
M	A(4+)				M	A(5+)			Mo	A(6+)	
	0.38	0.33	0.25	0.13	N	0.23	0.16	0.05	S	0.21	0.13
Si	0.5	0.46	0.4	0.31	P	0.37	0.31	0.23	Se	0.25	0.18
Ge	0.48	0.44	0.38	0.29	As	0.39	0.33	0.25	Te	0.33	0.26
Sn	0.52	0.48	0.43	0.35	Sb	0.43	0.38	0.31	Cr	0.27	0.2
Zr	0.54	0.51	0.46	0.38	Bi	0.44	0.39	0.32	Mo	0.29	0.22
Hf	0.54	0.5	0.45	0.37	V	0.39	0.33	0.25	W	0.29	0.22
					Nb	0.39	0.34	0.26			
					Ta	0.4	0.35	0.27			

for different elements. Evidently, for all fourfold coordination, the values of ionicity are the lowest and amongst these Si, Ge, C, P, As, Sb and Sn, which either form or contribute to a glass-forming network, have the lowest values of ionicity compared with those for the alkali metals in a sixfold co-ordination. In summary, a larger the value of ionicity of an element defines the localization of valence band electrons in a bonding.

The discussion on co-ordination shell and ionicity is relevant for engineering inorganic photonic glasses, especially those doped with either rare-earth or transition metal ions, in terms of explaining the short-wavelength absorption and cut-off, vibrational spectroscopy and the contributions thereof for optical transitions.

1.7 Definitions of Glass Network Formers, Intermediates and Modifiers and Glass-Forming Systems

In Figures 1.8a above a set of terminologies for oxides, namely the network forming, intermediates and modifiers, were introduced to help in identifying the roles of the oxides of metals and sub-metals that are often constituent parts of a glass structure. The discussions based on the partial charge on anions (Cl^-, O^{2-}) and ionicity of bonds and elements in Tables 1.3–1.5 explain the delocalization of valence electrons, which are essential in determining the "glass structure continuum and mechanical stability". On this basis, energetically the network formers are preferably those elements that have the lowest ionicity. In other words when such elements combine with oxygen atoms or halogens, a partial charge on the anion is left that is another manifestation of delocalization of valence electrons, defining their wave functions and overlap integrals with another like bond pair, e.g. O—Si—O, or O—Si—O—Na^+. It is immediately apparent how the delocalization of electrons on a Si—O pair would be affected, depending on the chemical nature of its environment. It is important to emphasize at this stage that a model based on electronegativity or ionicity has similarity with Philips's topological hypothesis [42] for chalcogenide glasses, which has been extensively discussed by Varsheneya [3]. The floppiness and deformability of chemical bonds in chalcogenide systems have been described by distinguishing the dominance of chemical and mechanical stabilities across the composition. The preponderance of "bond deformability and floppiness" has been ascribed as the glassy structure, and the lack of such continuum has been identified as "amorphous" state. Indeed, the deformability of a chemical bond is an intrinsic manifestation of "valence band electron delocalization" in a chemical bond.

Before explaining the types of glass-forming systems it is also important to consider the co-ordination shell for cations. Strictly speaking, since no cations form purely covalent or purely ionic bonds, analysis of the co-ordination shell in the realm of ionicity of cations or partial charge on anions becomes even more compelling. In brief this is summarized in Table 1.6 [32]. In this table, the valence band hybridization, e.g. sp, dp, sp^2, dp^2 etc., is shown leading to a specific topological description, with the smallest R_c/R_A yielding structures such as trigonal pyramid, tetrahedron, square planar and bipyramid. For example, in a silicon–oxygen bond pair, the electronic structures of silicon and oxygen are [Ne]$3s^2 3p^2$ and [He] $2s^2 2p^4$, respectively; as a result, we expect that (p_x^2, p_y^1, p_z^1) electron wave functions from oxygen will interact with the (p_x^1, p_y^1) wave functions from silicon. The process of hybridization is comparable with what happens in a diamond or a methane structure. The silicon hybrid forms by donation of one electron from the $3s^2$ level of silicon to an empty p_z state, which then creates four unpaired states $3s^1 3(p_x^1, p_y^1, p_z^1)$. Once this metastable transition occurs only then can the four electrons in 2p level from oxygen combine and yield an sp^3-type hybridization in SiO_2. The sp^3 hybridization is an intrinsic characteristic of group IVB elements; consequently, strong covalent bonds form with tetrahedron symmetry, having bond angles close to 109.5°. The above hybridization is the basis for the $(SiO_4)^{4-}$ structure in

Table 1.6 *Co-ordination number, minimum radius ratio, orbitals and geometrical structures [32]. Source: J. H. Simonns 1991. Reproduced with permission from Academic Press, San Diego.*

Co-ordination number	Minimum radius ratio (R_C/R_A)	Orbital hybridization	Resulting geometrical structures
2		sp, dp	Linear chain
3	0.155	sp^2, ds^2	Trigonal planar
		p^3, d^2p	Trigonal pyramid
4	0.225	sp^2d, p^2d^2	Square planar
		sp^3, d^3s	Tetrahedral
		d^4	Tetragonal pyramid
5	0.155	sp^3d, d^3sp	Trigonal bipyramid
6	0.414	d^2sp^3	Octahedron
		d^4sp	Trigonal prism
7	0.592		1 atom above the face of an octahedron
8	0.645	d^4sp^3	Dodecahedral square
	0.732		Antiprism, cube
9	0.732		Right triangular prism
12	1.00		Cube, octahedron

silica and silicate glasses. Similarly, in case of phosphate $(PO_4)^{3-}$, which also has a tetrahedron structure, is a part of hypervalent molecular structure. A hypervalent structure "is a molecule that contains one or more main group of elements, formally bearing more than eight electrons in their valence shells". In this case the hybridization of wave functions is sp^3d, which is why one of the phosphorus oxygen bonds is a double-bond, resulting in a (PO_4) structure. On the other hand, boron–oxygen bonding is predominantly sp^2 (co-planar) following carbon's graphite-like arrangement in a $(BO_3)^{3-}$ trigonal pyramid, whereas in the $(BO_4)^{5-}$ tetrahedron structure the hybridization is more complex than the plain sp^3 hybridization in an $[SiO_4]^{4-}$ structure.

Examples of electronic hybridizations resulting in specific topologies are shown in Figure 1.9. Complex hybridizations, namely d^4sp^3 etc., resulting in larger co-ordination numbers yield more complex shapes than octahedron, for example. Antiprisms and dodecahedra are such examples, which are often manifested by strong electropositive cations and tri- and divalent lanthanides.

1.7.1 Constituents of Inorganic Glass-Forming Systems

In this section our main aim is to classify different types of inorganic glass-forming systems by identifying the co-ordination chemistry of the main constituent that contributes to the network formation. The method of classification based on co-ordination number of central atom bonded with anions in a structural unit allows us to visualize the pervasiveness of the three-dimensionality of a specific network former. On this basis it is easier to identify the glass-forming systems into the following categories:

(a) Glass-forming networks based on cations of B, Si, P and Ge and oxide ion as anion (O^{2-}). These are *strongly covalent* glasses, as is apparent from the electronegativity, partial

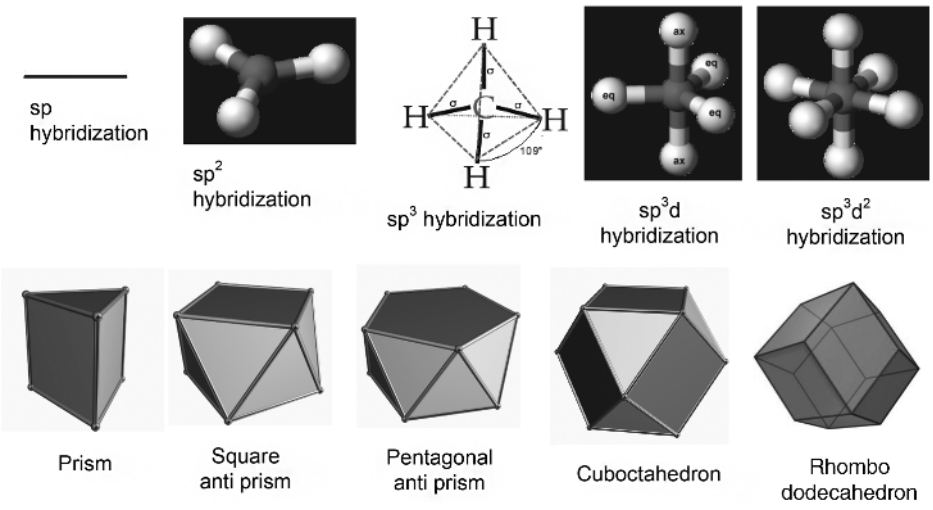

Figure 1.9 *Illustrations of common electronic hybridizations (sp, sp^2, sp^3, sp^3d, sp^3d^2) and higher orders of hybridization resulting in energetically favoured geometrical shapes, e.g. prism, antiprisms, cube octahedron and rhombo-dodecahedron [43]. (See colour plate section.)*

charge of oxide ion and ionicity of bonds, discussed in Tables 1.2, 1.4 and 1.5, respectively.

(b) Glass-forming systems based on heavy-metal oxides that have significant ionic character but are not as ionic as the electropositive elements of groups IA and IIA in the periodic table. These are glasses based on the oxides of aluminium, gallium, tellurium, vanadium, niobium, tantalum and tungsten, and are also known as the *conditional glass-formers*, which means that the liquids of pure compounds require either another network modifying oxide or another network-forming component oxide for the stabilization of glass structure.

(c) As the oxygen and fluorine atoms are comparable in size and in their values of electronegativity there is also a group of fluorides that forms glass. They are based on the fluorides of Be, Zn, Cd, Al, Zr, Hf and Th. A vast majority of pure fluorides of these elements, except that of Be, are also conditional glass-formers and need either another fluoride or oxide to stabilize the glass-forming liquids, as exemplified above in Section 1.4 in Figures 1.5 and 1.6. Amongst fluoride glass-forming systems, there are also mixtures of fluorides with oxides in which a limited range of composition forms a glass. Typical examples are mixtures of silicates and aluminium phosphates with the fluorides of group IA, IIA, IIB, IIIA and lanthanide elements. In contrast, the chlorides and bromides do not mix well with oxides, and therefore do not contribute to glass formation. However, several mixtures of chlorides, bromides and iodides are known in the literature for glass formation.

(d) Since the atoms of carbon, nitrogen and oxygen have comparable atomic size, these elements, with silicon and aluminium especially, form glass when precursor compounds such as Si_3N_4, SiO_2, Al_2O_3, AlN and SiC are mixed and melted above 1700 °C in an atmosphere of argon or nitrogen. The combination of oxides and nitrides of silicon and aluminium forms a tough glass and glass ceramic called SiAlON, an acronym derived

from the elements involved in its constitution [44,45]. On the other hand, mixtures of oxides and carbides are known to yield an oxycarbonitride glass [46], which might be a mixture of phase separated regions of the sp^3 hybridization of Si—C, Si—N and Si—O bonds, yielding a dark grey glass. The quality of such glasses is often quite poor due to rapid evolution of carbon dioxide and carbon monoxide gases during melting under the atmosphere of nitrogen or argon gas. The oxycarbide compositions, as a result, are not well studied.

(e) The final group of inorganic elements, where glass formation is commonly observed, is the chalcogenide elements, namely S, Se, Te and their compounds, especially with the group elements IIIA, IVB and VB. Extensive ranges of glass formation have been reported in the literature along with their optical, electronic and mechanical properties. In selected chalcogenide glass-forming systems, partial substitution of chalcogenide elements with halogens such as the chlorine, bromine and iodine have also been reported, leading to compositions called "chalcohalides", a new hybrid name coined to represent the chemical composition.

1.7.2 Strongly Covalent Inorganic Glass-Forming Networks

As explained above, the glass-forming networks in this family of compositions are the oxides of silicon, boron, phosphorus and germanium. Silica based glasses are derived either from melting or sol–gel processing of precursors of silica with modifying and intermediate oxide materials. Since the starting material is silica, it is important to compare the structure of crystalline silica and silicates with the corresponding glass compositions, especially when other network forming oxides, intermediates and modifiers are mixed to form a glass by melting the starting crystalline materials.

The quartz crystal is the commonest form of crystalline silica, which also occurs in nature. In the crystalline form, a Si^{4+} cation is in a tetrahedron co-ordination with four oxygen (O^{2-}) ions, which is represented as a $[SiO_4]^{4-}$ tetrahedron. In crystalline form the $[SiO_4]^{4-}$ structure repeats itself over an infinitely long three-dimensional space with each fourfold co-ordinated silicon surrounded by two O^{2-}ions on either side, which is how the entire network of $[SiO_4]^{4-}$ tetrahedron repeats itself. The O—Si—O bonding is called the "bridging oxygen" and only on the surface of crystals is the bridge broken, which is identified as the "non-bridging oxygen". In liquid and glassy silica, the first major difference is the absence of a three-dimensional periodic structure (Figure 1.10a). Figure 1.10b shows the $[SiO_4]^{4-}$ tetrahedron with the corresponding Si—O and O—O distances, which depend on crystalline, glassy and liquid forms of silica. By comparison, Figure 1.10c shows an example of α-tridymite, one of the polymorphic forms of crystalline silica; it represents the three-dimensional periodicity for which the two-dimensional representation is also compared in Figure 1.10a. Figure 1.10d shows a 2D representation of a 3D-dimensional network of glass structure that is random, which implies that with respect to a point of reference the space groups do not repeat periodically in any direction. However, a regular pattern of a hexagonal ring structure in Figure 1.10a has changed to polygonal rings in a corresponding glassy structure in Figure 1.10d. In this figure a significant number of non-bridging oxygen sites around the structure of silica glass is shown to have terminated at the edge of structure. In Figure 1.10e the structure of silica glass is further modified by the presence of monovalent sodium ions (Na^+) in the structure. As explained above in the context of electronegativity and

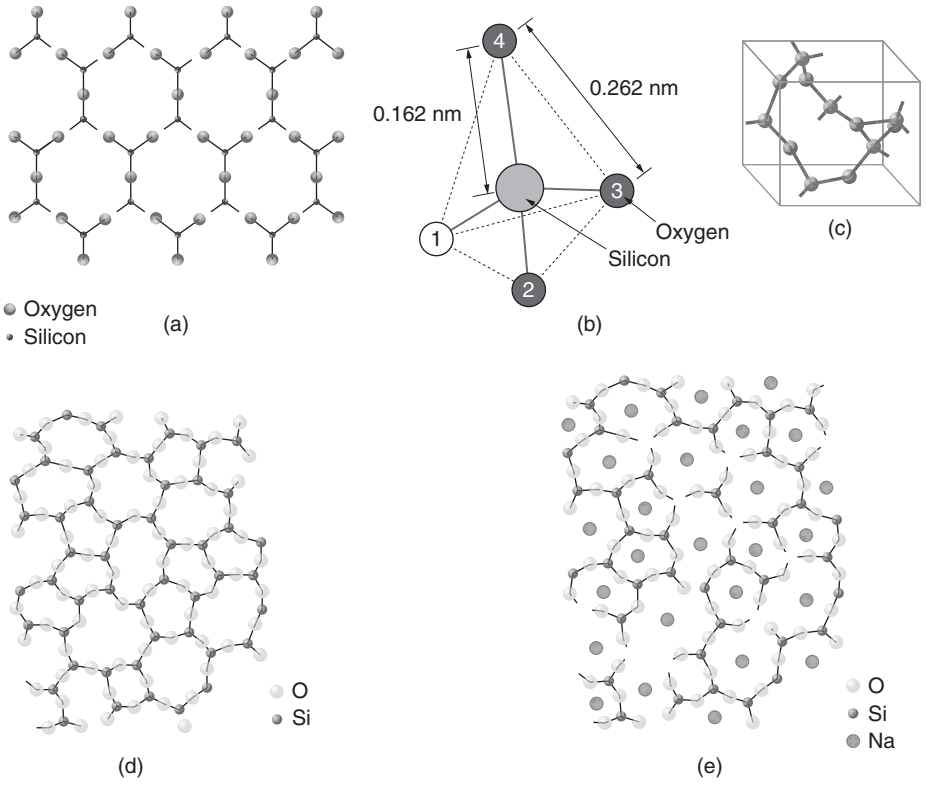

Figure 1.10 *Schematic representations of (a) a coplanar representation of the 3D-periodic array of sp^3 hybridized Si—O bonds, in which the fourth oxygen ion (O^{2-}) is perpendicular to the plane of the paper, as shown in (b); (b) a tetrahedron $(SiO_4)^{4-}$ structure of silica, which is the main building block in both the crystalline and amorphous (glassy) states; (c) the crystalline tridymite structure of SiO_2, which forms a 3D periodic continuum; (d) a 3D continuous aperiodic structure of silica glass showing bridging oxygens between two silicon atoms and the non-bridging oxygen anions at the edges which have only one silicon; (e) a sodium ion (Na^+) modified silica glass network in which Na^+ creates a more open structure by producing more non-bridging oxygen compared with the structure of pure silica glass in (d). (See colour plate section.)*

ionicity factors affecting an inorganic structure, monovalent cations tend to have a large co-ordination environment, which suggests that in order to incorporate an alkali ion the neighbouring bridging bonds between Si and O will have to terminate internally to create surfaces, as shown in Figure 1.10e. The incorporation of alkali ions in a silica matrix creates non-bridging bonds via the reaction shown in Equation 1.14, which can be adopted for other types of network formers:

$$y\left[\dot{:}\text{Si—O—Si}\dot{:}\right] + \text{M}_x\text{O}_y = y\left[\dot{:}\text{Si—O}^-\right] + x\text{M}^{y+} \qquad (1.14)$$

In this equation, "$\dot{:}$" designates the three electrons on silicon in the formula unit that also form Si—O bonds in a tetrahedron shown in Figure 1.10b. Evidently, a modifying oxide breaks y

number of Si—O bridging bonds, and therefore creates the non-bridging bond sites in Figure 1.10e. Such internal bond cleavage has major consequences for the spectroscopic, mechanical and physical properties of most covalently bonded glass networks.

With this brief introduction to silica and silicate glass structure, our focus in the rest of this chapter will be to discuss various compositions of silicate, phosphate, borate and germanate glasses. We will then return to the structural analysis of each type of glass in Chapter 2.

Table 1.7 shows the composition ranges for glass formation in borates, silicates, germanates and phosphates. The experimental conditions adopted for determining the glass forming compositions are stated briefly.

Table 1.7 *A list of glass-forming composition range, (m) identifies the presence of miscibility gaps in silicates [1,47]. Data from [1] and [47].*

Metal oxides that modify or contribute to a glass network	Covalently bonded network oxides			
	B_2O_3 [a]	SiO_2 [b]	GeO_2 [c]	P_2O_5 [c]
Monovalent oxides				
Li_2O	100.0–57.3	100.0–64.5	100.0–76.2	100.0–40.0
Na_2O	100.0–62.0 33.5–28.5	100.0–42.2	100.0–62.0	100.0–40.0
K_2O	100.0–62.3	100.0–45.5	100.0–40.5	100.0–53.0
Tl_2O	100.0–55.5	—	100.0–52.5	100.0–50.0
Divalent oxides				
MgO	57.0–55.8	100.0–57.5 (m)	Unknown	100.0–40.0
CaO	72.9–58.9	100.0–43.3 (m)	84.5–64.5	100.0–40.0
SrO	75.8–57.0	100.0–60.0 (m)	86.0–61.0	100.0–46.0
BaO	83.0–60.2	100.0–60.0 (m)	100.0–90.0 82.5–70.4	100.0–42.0
ZnO	56.0–36.4	~2	100.0–52.0	100.0–36.0
CdO	60.9–45.0	Unknown	Unknown	100.0–43.0
PbO	80.0–23.5	0–60	100.0–43.0	100.0–38.0
Trivalent oxides				
Bi_2O_3	78.0–37.0	Up to 60	100.0–66.0	95.0–70.0
Al_2O_3	Not known	0–10	100.0–95.0	75.0–68.0
Tetravalent oxides				
TiO_2	Not known	Not known	Not known	60.0–35.0
TeO_2	20.0–40.0	limited	Up to 90.0	100.0–1.0
Pentavalent oxides				
V_2O_5	90.0–10.0	<5	Not known	Wide range
Nb_2O_5	90.0–10.0	<5	Not known	>95.0
Ta_2O_5	80.0–70.0	<5	Not known	—

[a] All boric oxide based precursor materials were batched between 1 and 3 g in size. The mixture was melted in a platinum crucible and after homogenization it was allowed to cool naturally in air.

[b] Each silicate batch size was between 1 and 2 g in size, and was melted in air and cooled naturally to room temperature, as described in footnote *a*.

[c] For germanium oxide and phosphate glasses, the batch size was between 1 and 3 g, and was melted and quenched as above in footnotes *a* and *b*.

In the binary composition, the composition range for the main component is cited. For example, with Li_2O as a second constituent in four glass forming networks, the composition of Li_2O varies between 0 and 47.7 mol.% in B_2O_3, 0 and 35.5 mol.% in silica, 0 and 23.8 mol.% in GeO_2 and 0 and 60 mol.% in phosphate liquid. In the table, the composition ranges of miscibility gaps are identified by (m), which are prevalent in silicates. Briefly, the miscibility gap is a region of composition where the constituent phases tend to physically separate in the frozen state. These may be the sub-liquidus and sub-solidus miscibility. Alternatively, the regions of immiscibility may exist in the liquid state, too, the principles of which explained by examples in subsequent chapters with reference to the properties of glass ceramics used for photonic devices.

In Table 1.7, a large number of oxides in the first column are listed that are known to dissolve in the matrix of network formers, and yield binary compositions. What is apparent from the list is that, as the cationic charge on solute oxides increases, such oxides become structurally and energetically incompatible in the network forming matrices, and promote phase separation and crystallization.

1.7.3 Conditional Glass Formers Based on Heavy-Metal Oxide Glasses

Amongst the oxide compounds, such as Al_2O_3, Ga_2O_3, TeO_2, V_2O_5, Nb_2O_5, Ta_2O_5, MO_3 and WO_3, that cannot form glass on its own and rely on the presence of other constituent oxides or similar compounds, the tellurium oxide compositions have been most extensively studied. Since these glasses rely on other constituent oxides to be present in the liquid for glass stability, these oxides glasses are the so-called "conditional" glass-formers. Among the trivalent Al_2O_3 and Ga_2O_3 glass-forming networks are the pseudo-ternary compositions that have been reported by Mazurin and co-workers [47]: Al_2O_3-$(Na,K)_2O$-TiO_2, Al_2O_3-$(Na,K,Cs)_2O$-$(Ta,Nb)_2O_5$, Al_2O_3-(Cd,Pb)O-Bi_2O_3, Al_2O_3-La_2O_3-CaO and Al_2O_3-BaO-TiO_2. These aluminate compositions were melted in a platinum crucible at 1500 °C in air for 30 min, and the liquid was quenched onto a stainless steel surface. The glass-forming compositions in gallium oxide are: Ga_2O_3-$(Na,K,Cs)_2O$-Ta_2O_5, Ga_2O_3-$(K,Cs)_2O$-Nb_2O_5, (Ga_2O_3:La_2O_3-CaO = 40 : 40 : 20 by wt%) and Ga_2O_3:Bi_2O_3-(Ca,Sr)O, which can be melted in the temperature range 1250–1400 °C. The glass-forming range is often limited in these ternary compositions and requires an extensive cooling rate. By comparison, when alkaline earth metal oxides are replaced by CdO, PbO and ZnO, the melting temperature for glass fabrication drops to 1000 °C, as reported by Dumbaugh [48]. It is claimed in the reference that the bismuth-lead-gallium oxide glasses can be melted at 1000 °C in air for more than 20 min and up to 200 g batches were cast using this method of melting. As an example, we show a ternary section to represent the composition map for glass formation in the $GaO_{1.5}$-$BiO_{1.5}$-PbO ternary in Figure 1.11. The aspects of co-ordination number of Al^{3+} and Ga^{3+} and their structures will be discussed in Chapter 4.

Tellurium oxide (TeO_2) falls in the category of a conditional glass-former, as it was first identified by Stanworth [49] in 1952. The tellurite family of glasses has been widely reported by many authors and amongst the earliest works by Imaoka and Yamazaki [50], Dimitriev and co-workers [51,52], and Vogel and co-workers [53]. Besides Vogel, who examined especially binary compositions listed in Table 1.8, a vast majority of previous results on the physical and chemical properties of ternary tellurite glasses were based on the mixtures of alkali, alkaline earth, sesquioxides and other higher valency oxides. Among the inorganic

Table 1.8 *List of binary composition ranges in the tellurite family of glasses [47,51]. Data from [47,51].*

Metal oxide	Composition range (mol.%)	Metal oxide	Composition range (mol.%)	Metal oxide	Composition range (mol.%)	Metal oxide	Composition range (mol.%)
Univalent oxides		**Divalent oxide**		**Trivalent oxides**		**Higher valency oxides**	
Li_2O	12.2–34.9	BeO	15.0–27.0	Al_2O_3	7.6–16.8	TiO_2	6.2–18.9
Na_2O	5.5–37.8	MgO	11.0–35.0	La_2O_3	4.5–9.5	ThO_2	5.2–11.0
K_2O	6.5–19.5	CaO	<10.0	Ga_2O_3	0.0–20.0	P_2O_5	0–50.0
Rb_2O	5.6–21.0	SrO	9.2–13.1	Bi_2O_3	0.0–5.0?	V_2O_5	0–50.0
Tl_2O	13.0–38.4	BaO	8.0–35.7	In_2O_3	<5.0	Nb_2O_5	2.2–24.0
Cs_2O	0–10.0	ZnO	17.3–37.2	Sc_2O_3	<5.0	Ta_2O_5	1.4–15.3
Ag_2O	30–50.0 wt%	PbO	12.8–22.6	Y_2O_3	<5.0	WO_3	8.5–44.0
		CuO	12.0–36.0	Gd_2O_3	~3.0		
		CdO	0.0–5.0	As_2O_3	~3.0		
				B_2O_3	0–15.0		

glasses known today, the tellurite family of glasses are unique in structure, as they are based on three different types of structural polyhedrons of Te^{4+} ions [51], namely the trigonal bipyramid $[TeO_4]^{4-}$, trigonal pyramid $[TeO_3]^{4-}$ and polyhedron $[TeO_{3+x}]^{4-x}$. Each structural unit has a lone pair electron site, which contributes to the unique spectroscopic properties of these glasses – a subject area for discussion in Chapters 4 and 6. In the tellurite

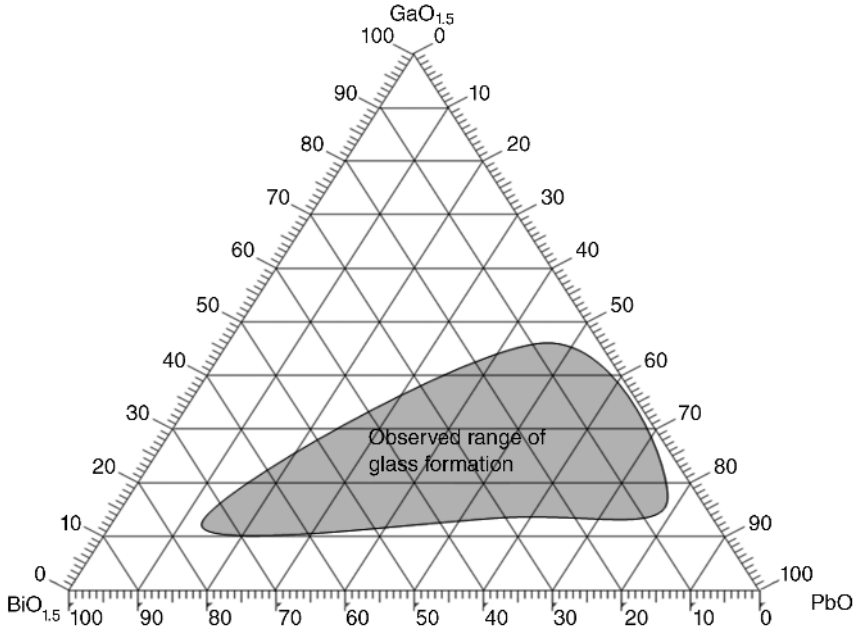

Figure 1.11 *Composition mapping of glass formation in the Ga_2O_3-Bi_2O_3-PbO system, which is represented as a $GaO_{1.5}$-$BiO_{1.5}$-PbO section. Source: W. H. Dumbaugh 1986. Adapted with permission from Society of Glass Technology.*

family of glasses one property that is frequently manifested is the mixing properties with another glass forming networks such as the borates, phosphates, silicates, germanates, niobates, tantalates, molybdates and tungstates. A binary tellurite can also mix with another chalcogenide oxide, such as the $(SO_4)^{2-}$ and $(SeO_4)^{2-}$ complexes. The compositions stated in Table 1.8 have been compiled from different sources and represent a reasonable selection of binary oxides.

Several scores of ternary tellurite composition maps with their physical and chemical properties have been compiled by Mazurin and co-authors [47]; they have formed the basis for applications of the reported compositions for device engineering.

Two different ternary composition maps are shown in Figure 1.12a and b, which define the TeO_2-Li_2O-R(Zn,Ba,Pb)O and TeO_2-Al_2O_3-R(Li,Na,K)$_2$O sections. These ternary compositions are one of the glass-forming systems investigated in detail for fibre and planar glass based device engineering.

1.7.4 Fluoride and Halide Network Forming and Conditional Glass-Forming Systems

The BeF_2 based glasses were the very first type of fluoride glasses, which were studied in the context of using the fluoroberyllate liquid as coolants for the fuel core in nuclear power plants. Beryllium fluoride has a similar structure to that of the $[SiO_4]^{4-}$ tetrahedron because the ratio of Be^{2+} and F^- ions is too small for the stabilization of structures, namely bipyramids and octahedral. Although the constituent anion F^- is ionic, the $[BeF_4]^{2-}$ structure is known to have strong covalent bond like features and is the only fluoride liquid that can form glass without the presence of a second constituent. Like silicate networks, the $[BeF_4]^{2-}$ network can also be modified by alkali fluorides, e.g. LiF, NaF etc., and can transform into a structure consisting of bridging and non-bridging F^- ion sites (Figure 1.10e). Zachariasen [27] first adopted his model for BeF_2 based glassed by describing the 3D-continuous random network. Baldwin and Mackenzie [54] developed a model for fluoride glass formation, based on Sun's bond model for fluorides and commented that

> "the essence of the relation of the single bond strength to glass formation is the assumption that the stronger-bonded constituent cations in a glass melt are less likely to have their bonds ruptured on cooling. A preponderance of strongly bonded cations will be less likely to undergo reordering as a prerequisite to crystallization and hence glass formation will be favoured."

Close examination of the Baldwin–Mackenzie model in the light of Sun's bond energy model points out that this model, like the electronegativity model, is fundamentally based on energetics and considers the preponderance of entropy of broken bonds leading to a glassy state, which we have discussed in Section 1.5.

For halide glass formation the anions from group VII are the main building blocks, as explained in Figures 1.3–1.6. These glasses can only be synthesized by chemical processes, e.g. melting, and are popularly known as the "halide family of glasses". Among these halide glass compositions, BeF_2 and $ZnCl_2$ are of no practical interest because of their hygroscopic nature, which renders them unsuitable for engineering applications. BeF_2 is also a carcinogenic material, however, it has some attractive optical properties, e.g. for a composition (weight percent) containing 26.0 BeF_2–18.0 AlF_3–27.2 CaF_2–29.7 NaF, the values of n_D and the Verdet constant are 1.3741 and 105, respectively, implying its low dispersion. It also has

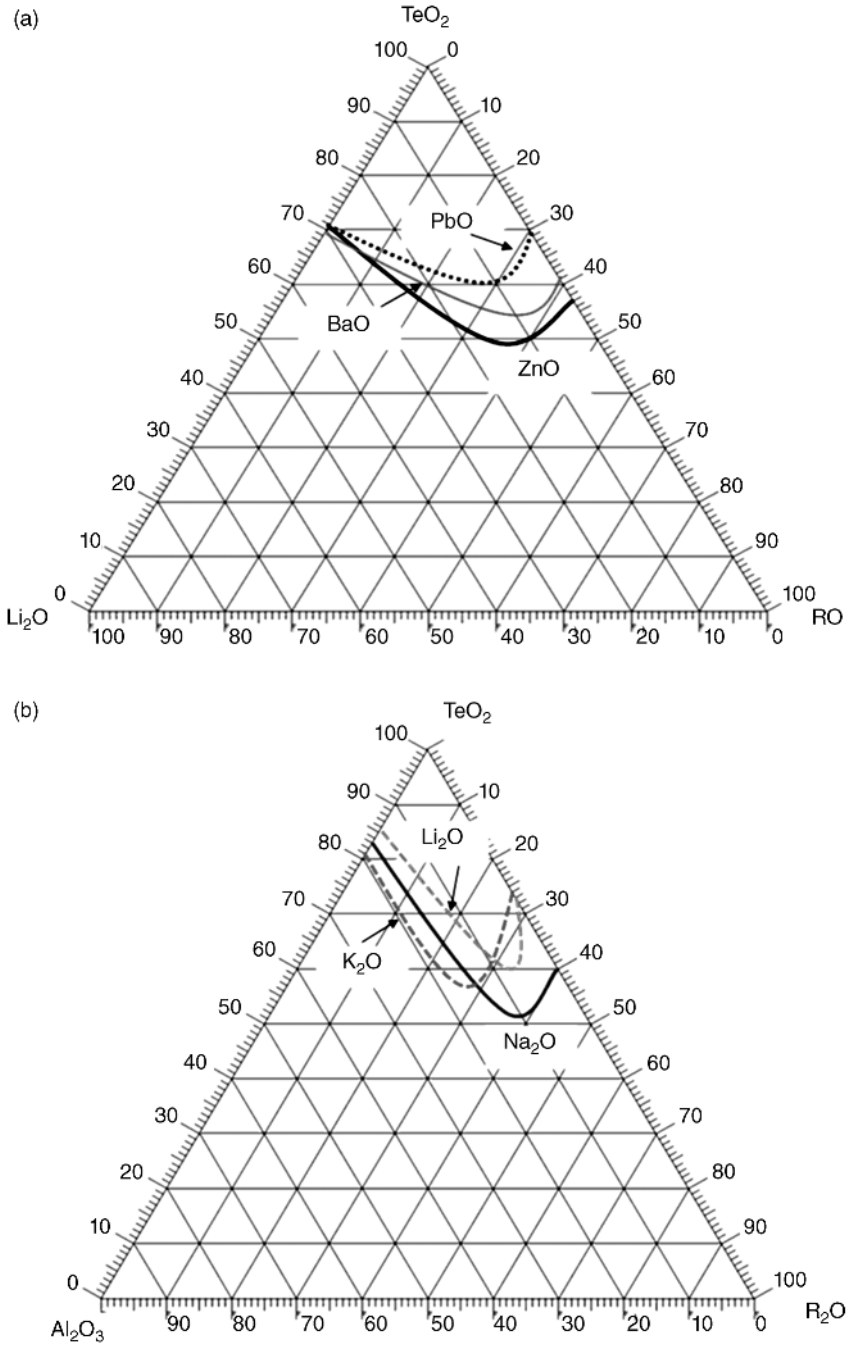

Figure 1.12 *(a) TeO_2-Li_2O-R(Zn,Ba,Pb)O and (b) TeO_2-Al_2O_3-R(Li,Na,K)$_2$O. These compositions were melted in gold-palladium crucibles at 800 °C in air [47]. Source: O. V. Mazurin 1991. Adapted with permission from Elsevier.*

low-loss window (<0.1 dB km^{-1}) that is at a longer wavelength that in silica. The BeF_2 glass has a low thermal expansion that is comparable with that of silica.

Besides the network formation in fluoroberyllate $(BeF_4)^{2-}$, zinc chloride and zinc iodide form glass networks based on the $[ZnX_4]^{2-}$ tetrahedron, which as in the liquid BeF_2 structure can be modified with the addition of alkali chlorides and iodides [55]. However, notably, these fluoroberyllate and zinc halide glasses are fundamentally hygroscopic, and extreme care is essential in reducing the incorporation of OH^- groups in the structure.

Trivalent and tetravalent fluoride glasses do not follow the Zachariasen model, as became apparent when they were serendipitously discovered by the Poulain brothers (Marcel and Michele Poulain) in 1975 [56], during their attempts to synthesize a sodium-barium fluorozirconate host for laser applications. The precursor powder when heat treated above 900 °C in air to synthesize the ternary crystalline compound yielded a glass instead (Figure 1.13).

A vast majority of these glasses are the "conditional glass formers" in the inorganic fluoride systems. In this section a series of conditional glass formers in halide systems are discussed along with their compositional maps. The most stable fluoride glass compositions were identified in a five-component mixture, having a nominal composition (mol.%) of $ZrF_4(55-x)$-$BaF_2(20-y)$-NaF(20)-$LaF_3(x)$-$AlF_3(y)$. These compositions have been studied extensively for device engineering, especially for fibre laser and amplifier engineering, which are also discussed in subsequent chapters. Table 1.9 reports significant compositions in the ZrF_4 based glass-forming systems. Following the serendipitous discovery of zirconium-based fluoride glasses, the University of Rennes I group in France further explored the analogues of fluorozirconate by partially and fully replacing zirconium with hafnium and studied their properties. The composition range of the thorium fluoride (ThF_4) family of glasses is much narrower than that in ZrF_4 and HfF_4 families of glasses. Besides the narrow range of stable composition of ThF_4 [57], for some compositions, e.g. ThF_4-BaF_2-LnF_3 [58], the quenching rate required is much higher than that in ZrF_4 and HfF_4 glasses. Here Ln represents the lanthanide elements in the periodic table. However, in barium-lithium thorium fluoride glasses (ThF_4-BaF_2-LiF) [59] and (ThF_4-BaF_2-LnF_3-AlF_3) [60] glasses much larger glass samples of several millimetre to centimetre sizes were cast for laser applications. Interestingly, the ThF_4 based compositions were reported to demonstrate much extended IR transmission than either ZrF_4 or HfF_4 [56]. However, the use of such glasses for engineering applications has been limited due to the radioactive nature of thorium.

Although several dozen fluoride and halide glasses have been explored and reported in the literature, very few have found their way to engineering applications and been drawn into fibres. Amongst them are the AlF_3-PbF_2-SrF_2-MgF_2 based glasses, originally reported by Sun in 1946 [61], which were further developed with and without the presence of phosphate in the form of sodium metaphosphate (Na_3PO_4). Videau *et al.* [62,63] systematically studied the ternary AlF_3-BaF_2-CaF_2 system, which were then stabilized by the addition of trivalent pre-lanthanide and rare-earth fluorides (YF_3, LnF_3) and drawn into optical fibres [64]. The compositions with phosphate group are especially interesting as it enhances the crystallization resistance and reduces the phase separation tendency. These fluoride glasses were also referred as the "Hoya" (a well-known Japanese Company) [65] glasses, which exhibit a lower refractive index than the standard silicates [66]. The combination of fluoride and phosphate in the glass network yields a unique feature of covalent and ionic bonding of $[AlF_n]$ polyhedral

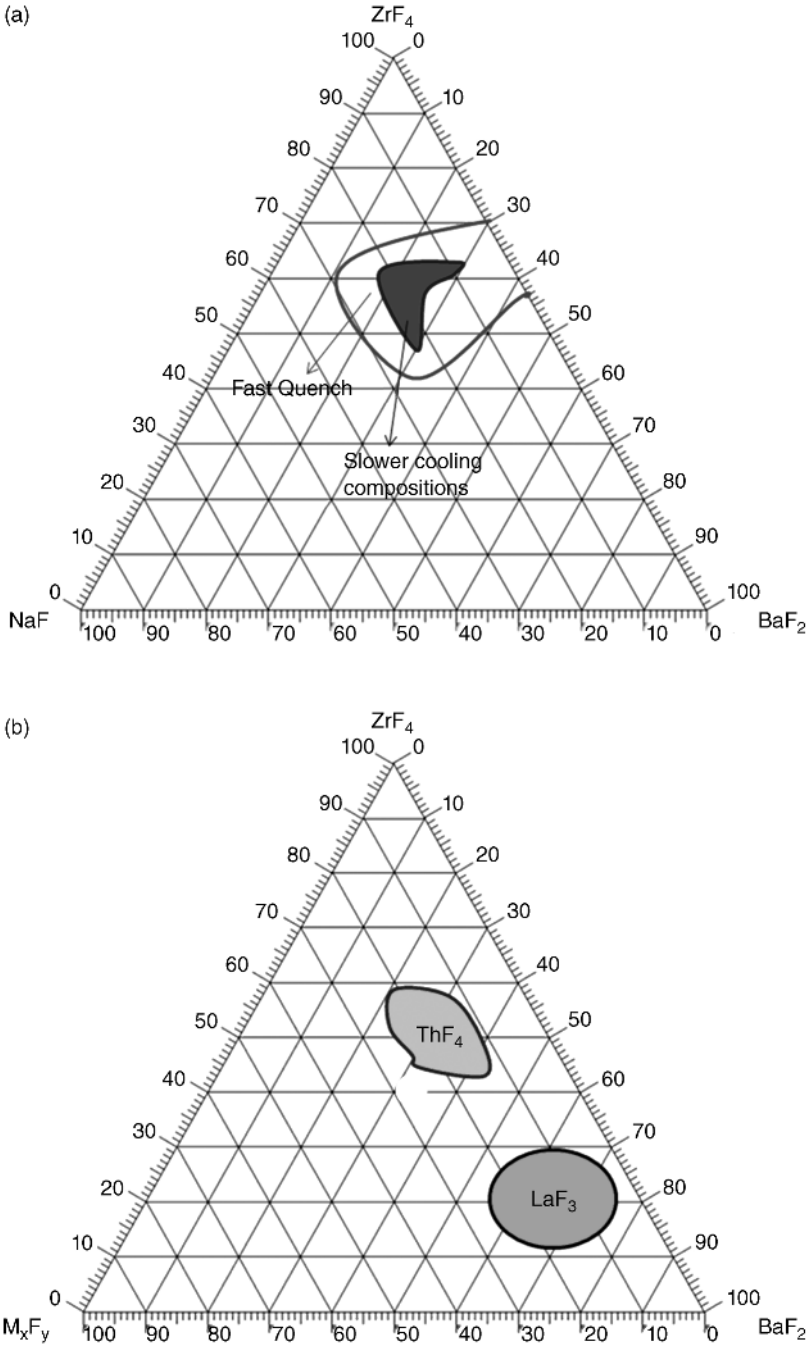

Figure 1.13 *Ternary composition maps for (a) ZrF_4-BaF_2-NaF and (b) ZrF_4-BaF_2-M_xF_y where M_xF_y designates the glass-forming composition range with LaF_3 and ThF_4. These compositions require quenching in air. The fluoride mixtures were heated in an atmosphere of dry air inside a platinum crucible at 850°C [25] before melting. Source: M. Poulain 1991. Adapted with permission from Academic Press, San Diego.*

Table 1.9 *List of compositions of tetravalent fluoride glasses with other minor fluorides [25].*

Acronym	Composition (mol.%)								
	HfF_4	ZrF_4	BaF_2	LaF_3	ThF_4	NaF	LiF	MFn	AlF_3
ZB		64	36						
HB	66		34						
ZS		70						$30SrF_2$	
HT	43				57				
ZP		70						$30PbF_2$	
ZBL		62	30	8					
ZBT		57	34		9				
ZBNa									
ZBN		60	34					$6NdF_3$	
ZBG		63	33					$4GdF_3$	
HBL	62		30	8					
HBT	60		33		7				
ZBNT		50	20		7.5	20			
ZBNT		50	20		7.5	22.5			
ZBLN		58	15	6		21			
ZBTLN		47.5	12.5	7	8	25			
ZTL		60		10	30				
ZTL		60		7	33				
ZTA		50			43				7
ZBLA		57	36	3					4
HBLA	58		33	5					4
ZBCA		60	32					$4CaF_2$	4
ZBYA		45	36					$11YF_3$	4
ZBNdA		60		28				$8NdF_3$	4
ZBGA		60.5	31.7					$3.8GdF_3$	4
ZBTA		57	29		10				4
ZBTLN		47.5	12.5	7	8	25			
ZBNA		52	24			20			4
ZBLiA		52	26				18		4
ZBLiLA		52	21	5			19		3
ZBLAN		57	18	3		17			5
ZBLAK		56	14	6				20KF	4
ZBLANK		56	14	6		10		10KF	4
ZBLANI		53	20	4		15		$4InF_3$	4

(tetrahedral, bipyramid and octahedron) and $Al(PO)_4$ tetrahedra, giving a preponderance of [AlF_n] polyhedral that are dependent on the presence of alkali, alkaline-earth and trivalent pre- and post-lanthanide fluorides [67]. Such structural features increase the crystallization resistance [68].

Analogues of AlF_3-based glasses and fibres are reported in the literature; they are based on GaF_3 and InF_3. Often these compositions were found to have large concentrations of oxygen in the form of oxides of In_2O_3 and Ga_2O_3. As evident from the Table 1.10 [25], these fluoride glasses often have combinations of one or more polyhedral structural units, as in AlF_n, which

Table 1.10 *List of compositions (defined in mol.%) of trivalent and divalent halide glasses [25,57]. Source: M. Poulain 1991.*

III A Fluoride	Pre-lanthanide fluoride	IV A Fluorides	IIA Fluorides	IIB Fluorides	IA Fluorides
40 AlF_3	16 YF_3	—	22 CaF_2, 12 BaF_2, 10 SrF_2	—	—
40 AlF_3	20 YF_3	—	20 BaF_2 and 20 CaF_2	—	—
30 AlF_3	20 YF_3	20 ThF_4	30 BaF_2	—	—
50 InF_3	—	—	20 BaF_2	30 PbF_2	—
40 InF_3	17 YF_3	—	32 BaF_2	11 PbF_2	—
45 GaF_3	—	—	—	25 PbF_2	30 KF
20 AlF_3	—	20 ThF_4	20 BaF_2	40 ZnF_2	—
—	—	—	30 BaF_2	40,30 Cd(F, $Cl)_2$	—
—	—	—	11 BaF_2	42,11 Cd(F, $Cl)_2$	36 NaCl

are essential for thermal stability. The lack of covalent structure in such glasses limits their thermal stability for optical fibre and waveguide engineering, which is why incorporating the $(PO_4)^{3-}$ units to balance the positive charge against $(Ga, In, Al)^{3+}$ provides thermal stability.

Some of these compositions will be discussed in detail in the context of glass preform and fibre fabrication and loss characterization.

1.7.5 Silicon Oxynitride Conditional Glass-Forming Systems

The oxynitride glasses are predominantly based on the co-ordination chemistry of Si and its interaction with oxygen and nitrogen. Silicon forms a stable nitride, called silicon nitride (Si_3N_4), and an oxynitride (Si_2N_2O). In both compounds the silicon atom is sp^3 hybridized with N and O giving an $[SiN_4]$ and an $[SiN_{4-x}O_x]$ tetrahedron structure, respectively. The oxynitride tetrahedron is also designated as an $Si(O,N)_4$ unit. Notably, however, Si_3N_4 on its own does not form a bulk glass and yet amorphous silicon nitride films are well known for their wide use in the microelectronics industry. It is for this reason that the family of oxynitride compositions are classed as "conditional glass formers". The propensity for glass formation, as expected from the knowledge in silicate systems, increases in the SiO_2-Si_3N_4 binary mixture when the network formers and contributors (B_2O_3, Al_2O_3) and modifiers (CaO, MgO, etc.) are added. The presence of such oxides not only lowers the glass formation but also expands the composition field, as has been explained in reviews on this subject [69,70].

Since the main components of glass-forming system are the oxides and nitrides of silicon and aluminium, these compositions are often used for engineering, e.g. a Y_2O_3 based yttrium-aluminium garnet oxide and nitride glass ceramic material (Figure 1.14). The example of a yttrium oxide based oxynitride glass is important in the context of investigating the solubility of rare-earth oxides in such a matrix. In addition, as the glass network is constituted from strongly covalent compounds, the ionic resistivity of O^{2-} ions is extremely large in these matrices, typically of the order of $10^{12}\,\Omega$ cm, which makes oxynitrides an interesting material for electrical poling in order to modify the refractive index.

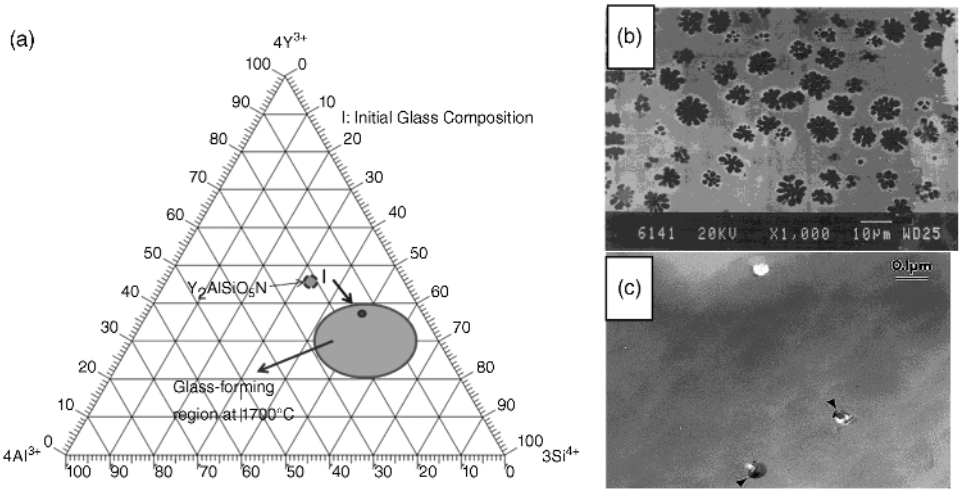

Figure 1.14 *(a) Y_2O_3 containing SiAlON glass compositions. The ternary composition shows the range of glass formation, which is designated by the large grey circle. The small dot inside the circle identifies the initial composition of the glass, with respect to the Y_2AlSiO_5N crystalline phase composition. (b) and (c) Transmission electron microstructures of crystallized SiO_2 [71] and silica-rich phase in the matrix of a Y-SiAlON glass [72], respectively. (b) Source: S. Hampshire 1994. Reproduced with permission from Elsevier. (c) Source: W. T. Young 2000. Reproduced with permission from Elsevier.*

1.7.6 Chalcogenide Glass-Forming Systems

The chalcogenide glass-forming systems are perhaps the most diverse with unique chemical, physical and spectroscopic characteristics. The unique and diverse characteristics are underpinned by the electronic configuration of chalcogenide elements which are the main constituent of this family of glasses. A chalcogenide glass-forming system *must* consist of one the elements from group VIB of the periodic table, excluding oxygen, which defines the oxide glass formers, discussed above. The main chalcogen elements are S, Se and Te. Individually when, for example, sulfur or selenium is melted and cooled rapidly, the element produces a glass. Sulfur also forms amorphous sulfur, which is not yellow but white in colour. Although the heaviest element polonium is also a chalcogen it is highly radioactive, which limits its use in engineering and technology. Selenium glassy materials were used in the old Xerox machines. The chalcogen elements also combine amongst themselves, e.g. Te and sulfur can be mixed together to form a glass.

One reason for their unique characteristics arises from the presence of a lone pair of electrons in the valence band orbital of a chalcogenide. As a result, a unique set of chemical characteristics is observed in the chalcogenide family of glasses, especially when the glasses are derived from the mixing of more than one chalcogen elements. Outside group VIB, chemical mixing via melting or other means with the elements of II(A,B), III(A,B), IV(A,B) and V(A,B) commonly yields a range of binary glasses, which are further stabilized when, for example, in a binary mixture of IIIB–VIB a third element from group IVB is mixed to make a ternary composition. Larger multicomponent compositions of chalcogenides can also be formulated. Such chemical combinations of chalcogenides predominantly form strong covalent bonds in the glass structure, although there are examples of less covalent structures such as those based

on Ga_2S_3, which also form glasses on rapid quenching, especially when mixed with La_2S_3 and GeS_2. These ionic bond dominated sulfide structures are conditional glass formers.

A vast majority of chalcogenide glasses follow the $(8-N)$ or "octet" rule, originally proposed by Professor Sir Neville Mott, who was rewarded with a shared Nobel Prize in Physics with Dr Phillip Warren Anderson at Bell Laboratories and Professor John Hasbrouck van Vleck at Harvard University for "their fundamental theoretical investigations of the electronic structure of magnetic and disordered systems". This groundbreaking discovery has since revolutionized microelectronics and now has an impact on nano-scale electronics, which can be found in Mott's Nobel lecture on "Electrons in Glass" [73]. This citation together with the classic papers authored by Ovshinsky [74,75] has opened up many applications of chalcogenide glasses. However, except for those compositions in thin film applications, many others have not yet reached fruition despite many years of research. Nonetheless a multitude of opportunities for utilizing these glasses for engineering applications lie ahead, which if achieved will bring about a new revolution in the entire field of photonics and optoelectronics. In this chapter the unique structural features are described for device applications of chalcogenide glasses.

Before describing the physical and spectroscopic properties of chalcogenide glasses, it is essential to identify the building blocks of glass-forming networks. This building block is very much dependent on the electronic structure of the elements which are briefly described below and is referenced from the original text book authored by Z U Borisova [76]. According to Borisova, the unary, binary and ternary glass forming structures are formed on the basis of the maximum allowable number of neighbours, which is determined by the valence bonds, which are as follows:

(a) Chains of selenium in a structural formula unit $SeSe_{2/2}$ are expected to exist in glassy Se structures, where $Se_{2/2}$ represents a bridging selenium with a neighbouring selenium in Figure 1.15a.

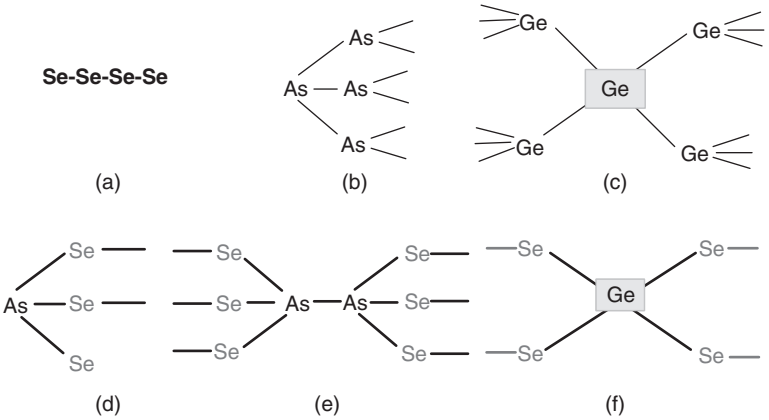

Figure 1.15 *Bonding in chalcogenide elemental and compound systems based on the valency: (a) Se-Se zig-zag linear chain; (b) trivalent chain in arsenic; (c) tetrahedron structure in sp^3 hybridized Ge atoms; (d) As-based trivalent chain in As-Se (e); and (f) tetrahedron $(GeSe_4)^{4-}$ structure [76]. Source: Z. U. Borisova 1981. Adapted with permission from Plenum Press.*

(b) In arsenic tri-chalcogenide systems the topographic distribution of bonds is as follows with the As $As_{3/3}$ network in Figure 1.15b.
(c) The valency of four in germanium determines the tetrahedron co-ordination (Figure 1.15c), with the spatial distribution of the units showing the Ge-$Ge_{4/4}$ network

The binary glass-forming systems with strong network formation can be designated by the hybridization of the group IVB and group VIB valence band electrons and are schematically shown as an example for selected selenium glass-forming systems. Both sulfides and tellurides can also be represented in a similar manner to the selenides shown in Figure 1.15d–f (respectively, As_2Se_3, AsSe and $GeSe_2$).

The schematic representations of chalcogenide glass-forming networks are consistent with structural analyses based on the electronegativity theory, discussed above. Many of these chalcogenide glasses exihibit strong covalency, especially when sulfur and selenium elements are involved in the glass-forming network. However, the covalency begins to diminish in such glasses as sulfur or selenium is replaced by tellurium.

Amongst the chalcogenide glass structures, described schematically in Figures 1.15a–f, there is a further opportunity to modify the glass structure by incorporating monovalent cations that occupy the sites around divalent selenium, for example, and form a network terminating site, as do the alkali ions in an oxide matrix. One of the divalent bonds at selenium at the edge of the structure preferentially becomes more negative and allows monovalent cations, such thallium, caesium, potassium and rubidium to occupy sites and terminate the network (Figure 1.16a). The incorporation of smaller cations such as sodium and lithium in selenide and telluride glass networks is more difficult due to their respective ionic sizes than in the sulfide glasses. A corollary of the structural modification using monovalent cations is the incorporation of monovalent anions such as iodide in the form of iodine. Since the chalcogenide elements are divalent, the iodine can share one of the divalent bonds and terminate the network (Figure 1.16b).

Selected examples of the ternary chalcogenide systems are shown in Figures 1.17a–f, in each of which the composition range for stable glass formation is mapped for comparative purpose. The details of complementary compositions can be found elsewhere in the literature [74]. Each of these compositions, however, represents the type of structural modifications we have discussed above in Figures 1.15 and 1.16.

The homopolar character of Ge, As, S and Se elements predominantly determines the magnitude of glass-formation regions in the Ge-As-(S,Se) systems shown in Figure 1.17a. The extended region of glass formation dramatically reduces when Se or S in the above

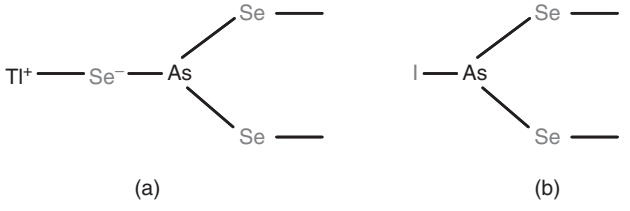

Figure 1.16 *Pictorial representation of structural modifications of an As-Se glass with monovalent ions: (a) thallium (Tl^+) and (b) iodine (I^-) anion [76] Source: Z. U. Borisova 1981. Adapted with permission from Plenum Press.*

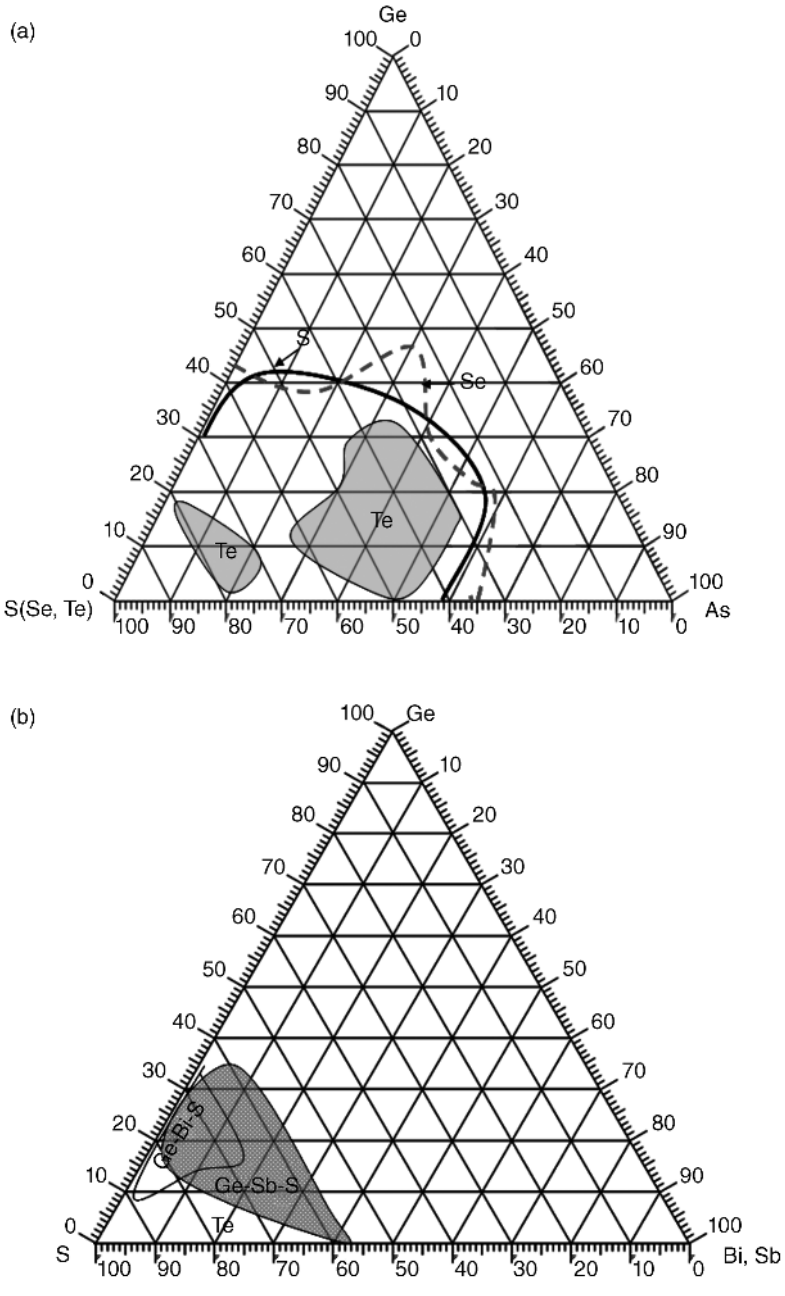

Figure 1.17 *Glass-forming composition maps: (a) Ge-S-As represented by the black solid line; Ge-Se-As by the broken light grey line; and Ge-As-Te by the two shaded regions. (b) Ge-S-Bi is depicted by solid continuous line; Ge-Sb-S as the shaded area [76]. (c) Glass formation in Ge-(Ga,In)Se. (d) Ge-(Sn,Pb)-Se-As glass forming systems. (e) Glass formation in (SiGe)-(Se)-I showing different regions of stabilities. (f) Ge-(As,Pb)-Tl-Se-As glass forming systems with different regions of glassy phase [76]. Source: Z. U. Borisova 1981. Adapted with permission from Plenum Press.*

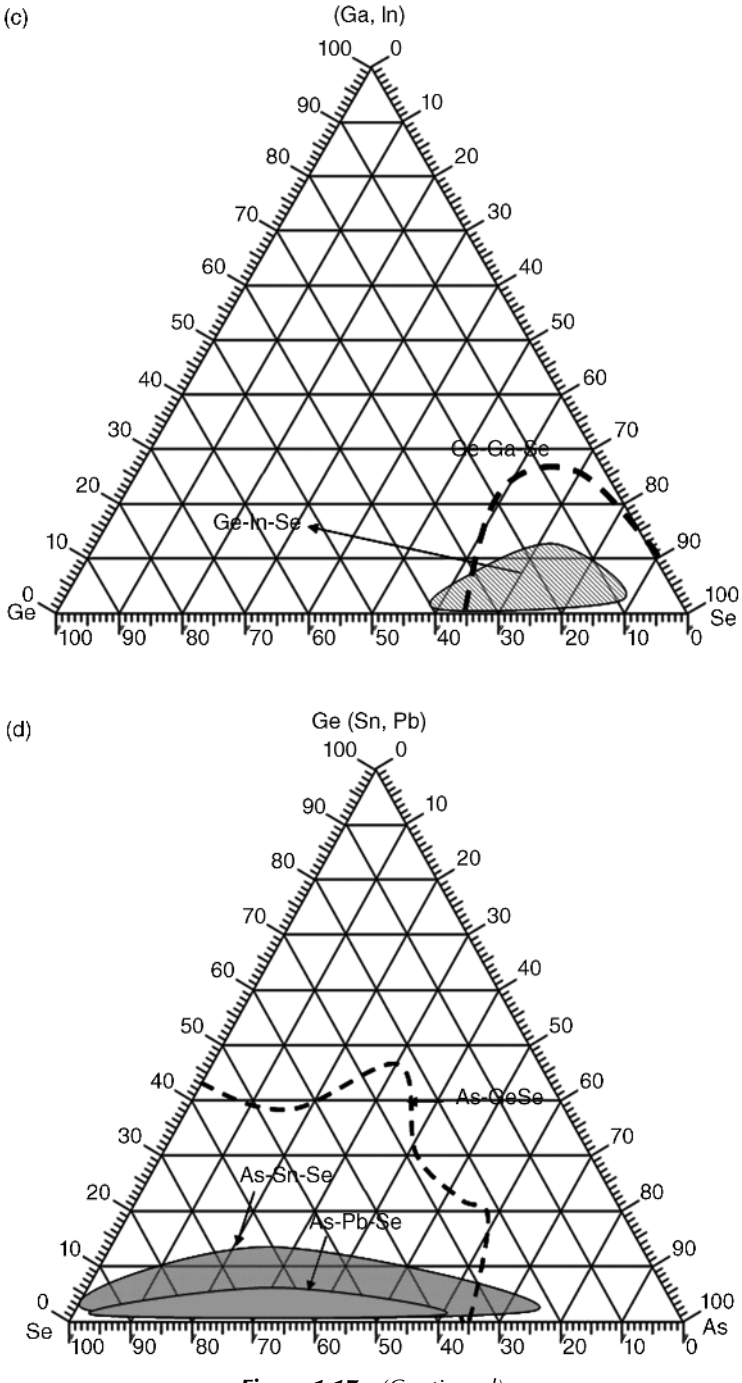

Figure 1.17 *(Continued)*

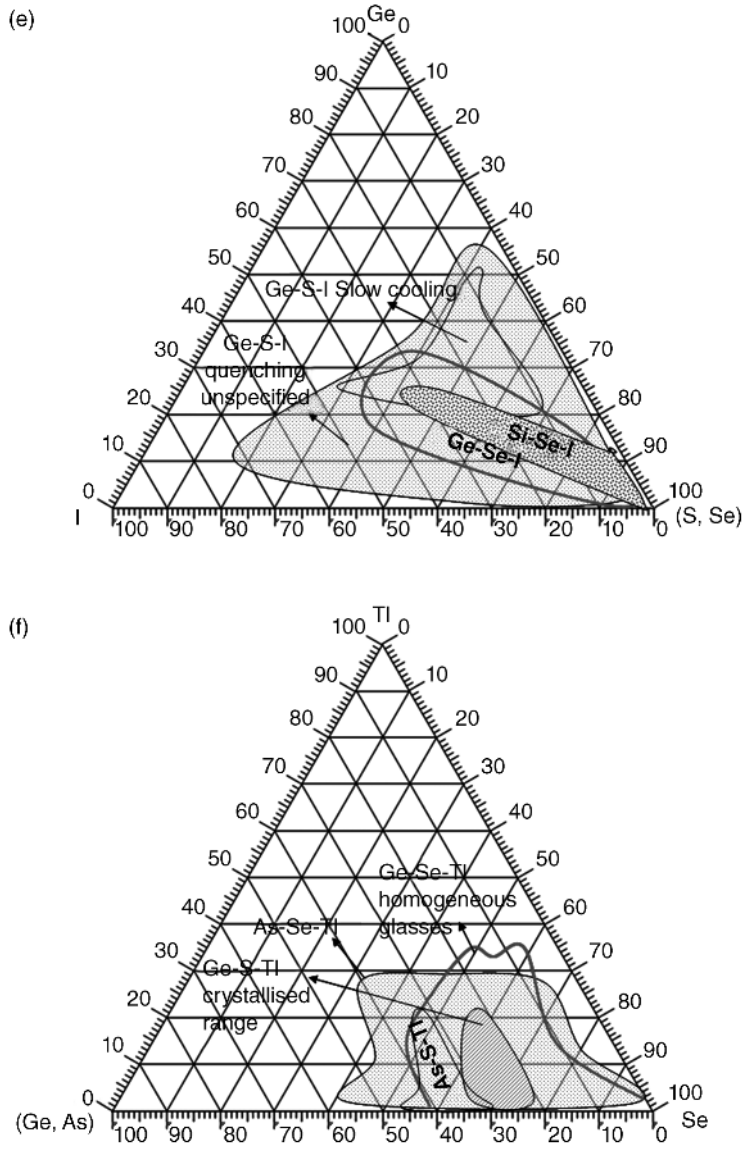

Figure 1.17 *(Continued)*

composition is wholly or partially replaced by Te, which is why in the Ge-As-Te system the region of glass-formation splits into two composition ranges. By contrast, in Figure 1.17b we see the influence of the lack of homopolar character of Bi and Sb on the glass-formation range in the (Bi,Sb-Ge-S) ternary, when As is replaced by Bi and Sb. The range of glass formation further reduces when Bi replaces Sb in the ternary, which may be attributed to the difference in the ionic or atomic radii of Bi and Sb.

The incorporation of gallium and indium as a third element in the Ge-Se binary, as shown in Figure 1.17c, introduces more ionic character, as opposed to homopolar bonding. The increase in ionicity is the consequence of a lack of sp^3 and sp^2 types of hybridization, which in the Ge-(Ga,In)-Se system can be increased by incorporating a proportionate amount of a group VB elements, namely P, As and Sb, so that the combination of III–V electronic hybridization yields an average of four electrons per sub-metallic element. Through this process of compositional modification, the sp^3 electronic hybridization may be enhanced in the glass structure.

As indicated in Figures 1.16a and b, the glass network sites in the chalcogenide structure encounter disruption when monovalent cations such as Tl^+ are incorporated into the glass-forming networks. Anions such as I^-, when they replace e.g. Se^{2-} in a chalcogenide structure, terminate the network sites. There is significant evidence from the composition map in Figure 1.17a that in the Ge-S-I ternary, although glass formation is more extensive than in either Ge-Se-I or Si-Se-I, the stable compositions requiring slow cooling are confined to a limited composition range. By contrast in Figure 1.17b, we see the influence of the lack of homopolar character of Bi and Sb on the glass-formation range in the (Bi, Sb-Ge-S) ternary, especially when Bi or Sb is replaced by As in Figure 1.17c. The range of glass formation further reduces when Bi replaces Sb in the ternary, which may be attributed to the difference in the ionic or atomic radii of Bi and Sb. The incorporation of gallium and indium as a third element in the Ge-Se binary, as shown in Figure 1.17d, introduces more ionic character, as opposed to the homopolar bonding. In Ge-Se-Tl the range of phase separation is quite apparent.

Although, potentially, several compositions might form glass by splat quenching in the chalcogenide systems, amongst the conditional glass-forming compositions the Ga_2S_3-La_2S_3 binary [77] (Figure 1.18) is the best known, especially due to the presence of La_2S_3,

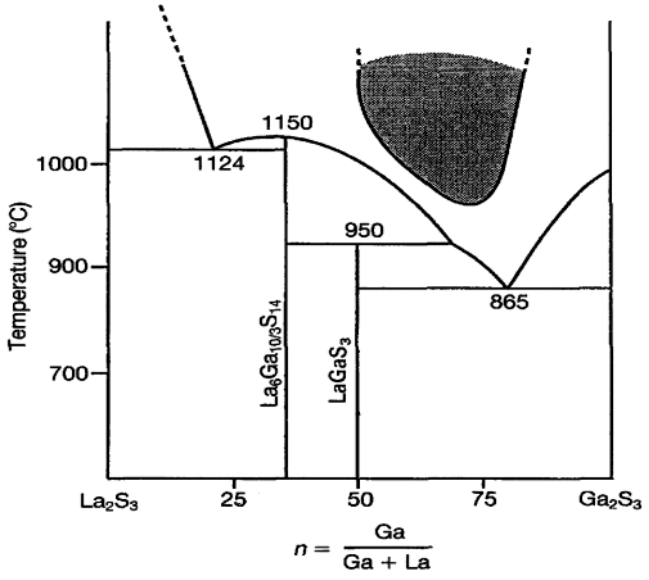

Figure 1.18 *Phase equilibrium boundaries and the glass-forming composition range in the Ga_2S_3-La_2S_3 binary system [77]. Source: Kumta, 1994. Reproduced with permission from Springer.*

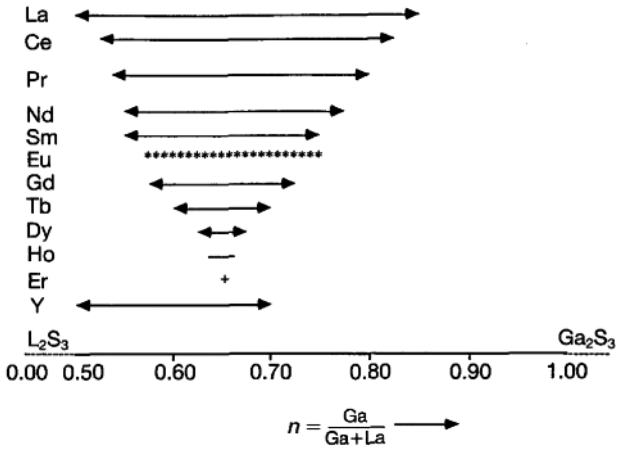

Figure 1.19 *Diagrammatic comparison of solubility limits of various lanthanides and yttrium (Y^{3+}) ions in the Ga_2S_3-La_2S_3 systems. Table 1.11 compares the ionic radii and atomic masses of various lanthanide elements [77]. Source: P. N. Kumta 1994. Reproduced with permission from Springer.*

which may be potentially substituted for other optically active rare-earth sulfides, as determined by the range of lanthanide sulfides investigated [78,79]. From these investigations, the trend in the solubility of rare-earth sulfides in the Ga_2S_3-La_2S_3 liquid seems to be quite size dependent, as shown in Figure 1.19, where we find that as the lanthanide ionic radius decreases with increasing atomic number the solubility range of rare-earth sulfide for glass formation also reduces. This decrease in solubility may be due to multiple co-ordination

Table 1.11 *Comparison of the ionic radii and atomic masses of lanthanide ions, indicating the contraction in ionic radius with increasing mass [80].*

Ionic radius (pm)	Atomic mass
$La^{3+} = 103.2$	138.905
$Ce^{3+} = 102$	140.116
$Pr^{3+} = 99$	140.907
$Nd^{3+} = 98.3$	144.242
$Sm^{3+} = 95.8$	150.360
$Eu^{3+} = 94.7$	151.964
$Gd^{3+} = 93.8$	157.250
$Tb^{3+} = 92.3$	158.925
$Dy^{3+} = 91.2$	162.500
$Ho^{3+} = 90.1$	164.930
$Er^{3+} = 89$	167.259
$Tm^{3+} = 88$	168.934
$Yb^{3+} = 86.8$	173.054
$Y^{3+} = 90$	83.905

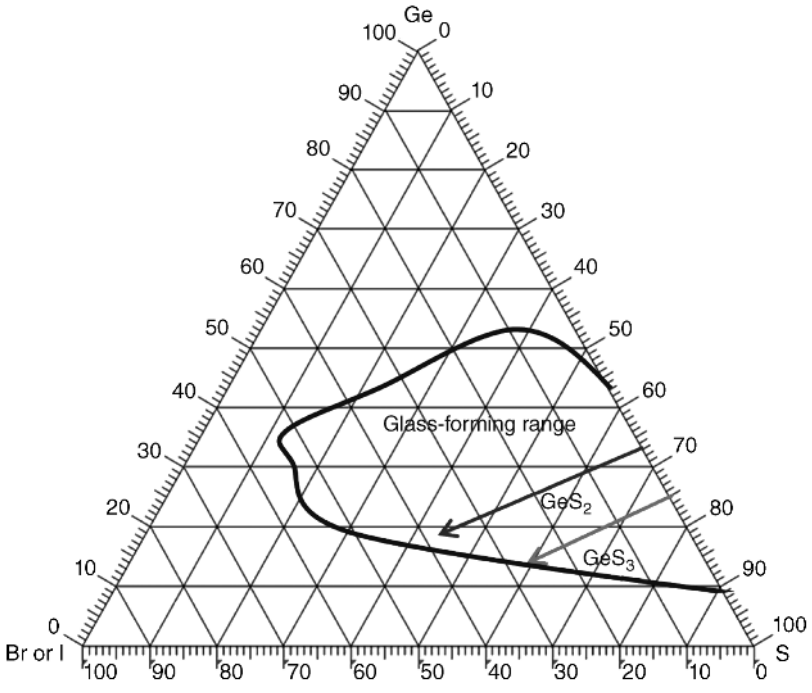

Figure 1.20 *Glass formation in the Ge-S-(Br,I) system, which falls between the GeS_2-GeS_3 binary Ge-S edge and extends towards the iodine anion (I^-) [82]. Source: S. A. Dembovskii 1971. Reproduced with permission from Springer.*

numbers (6–8) of higher lanthanides sulfides, compared with that of lower ones which have preferentially $z = 6$.

The multiplicity of co-ordination numbers in heavier lanthanides is reported by Wells [18b], where we find that the type C lanthanides (Er, Tm, Yb) may dwell in a large co-ordination field of up to eight by distorting the polyhedron. Since the gallium sulfide based structures are more ionic than the traditional sulfide, such distortions of co-ordination polyhedra might not be permissible due to geometrical constrains, which is why the heavier lanthanides tend to exhibit lower solubility in the gallium–lanthanum sulfide systems.

1.7.7 Chalcohalide Glasses

As discussed above from Borisova [74], the substitution of sulfur with iodine in a GeS_2 glass yields a non-bridging site where the iodide or bromide ions (I^- or Br^-) acts as bond terminators. Based on this model, Heo and Mackenzie [81] systematically examined the glass formation from an earlier investigation by Dembovskii *et al.* [82]. The S : I and S : Br ratio in the GeS_{2+X} (where $X = 0$ or 1) compositions were analysed and the resulting composition map is shown in Figure 1.20, in which the arrows depict the lines of constant Ge : S ratio, which vary between 2 and 3, corresponding to 66.7 and 75 at.% of S.

Many different types of chalcohalide glasses have been reported in the literature. A major review of compositions, properties and applications has been published by Sanghera and co-workers [83].

1.8 Conclusions

In this chapter the structural and thermodynamic background for the theory of glass formation is discussed along with examples that include both the covalent and ionic glasses. The compositions are discussed especially with reference to the known glass-forming range, which may be helpful for readers. Based on this background, in the following chapters the properties, fabrication and applications are discussed.

Selected Bibliography

1. A Paul, *Chemistry of Glasses*, 2nd edition (1990), Chapman and Hall (London).
2. S.R. Elliott (1984) *Physics of Amorphous Materials*, Longman.
3. A K Varsheneya, *Fundamentals of Inorganic Glasses*, 2nd edition, Society of Glass Technology (2006), Sheffield.
4. Z U Borisova, *Glassy Semiconductors* (Translated from Russian by J George Adhasko), Plenum Press (1981) New York.
5. R H Doremus, *Glass Science*, Wiley-Interscience, 1973 (1st Edition).

References

1. A. Paul (1982) *Chemistry of Glasses*, 2nd edn. Chapman & Hall, London, pp. 1–13.
2. J. Wong and C.A. Angell (1976) *Glass Structure by Spectroscopy*, 1st edn, Marcel Dekker, New York, ch. 1, pp. 1–51.
3. A.K. Varsheneya (2006) *Fundamentals of Inorganic Glasses*, 2nd edn, Society of Glass Technology, Sheffield, (a) pp. 281–283; (b) pp. 296–315.
4. S.R. Elliott (1984) *Physics of Amorphous Materials*, Longman.
5. A.E. Owen (1970) Semiconducting Glasses: Part-II on Properties and interpretations, *Contemporary Physics*, **11**, 257–286.
6. J. Jäckle (1986) Model of glass transition, *Reports on Progress in Physics*, **49**, 171–231.
7. W. Kauzmann (1948) The nature of glassy state and the behaviour of liquid at low temperatures, *Chemical Review*, **43**, 219–256.
8. O. Kubaschewski and C.B. Alcock (1979) *Metallurgical Thermochemistry*, 5th edn (Revised and enlarged), Pergamon Press, Oxford, pp. 268–339.
9. E.T. Turkdogan (1980) *Physical Chemistry of High-Temperature Technology*, Academic Press, London, (a) ch 1, pp. 5–25; (b) ch 2, pp. 26–35.
10. L.S. Darken and R.W. Gurry (1953) *Physical Chemistry of Metals*, McGraw Hill, New York.
11. R.A. Swalin (1972) *Thermodynamics of Solids*, Wiley-Interscience, New York.
12. F.D. Richardson (1974) *Physical Chemistry of Melts in Metallurgy*, Academic Press, London. (a) pp. 133–139; (b) pp. 205–213.
13. C.H.P. Lupis (1983) *Chemical Thermodynamics of Materials*, Elsevier Science Publishing Company.
14. M.F. Ding, J. Lau, and J.D. Mackenzie (1986) Halide glasses based on chloride, bromide and iodides, *Journal of Non-Crystalline Solids*, **80**, 538–542.

15. W.D. Kingery, H.K. Bowen and D.R. Uhlmann (1976) *Introduction to Ceramics*, 2nd edn, John Wiley & Sons, New York.
16. J. Hulme, A. Jha, J.M. Parker, and A. Whitehouse (1989) Formation of far-IR transmitting AgI-CsI glasses, *Physics and Chemistry of Glasses*, **30**, 254–259.
17. C. Brink, N.F. Binnendijk, and J. Van de Linde (1954) The crystal structures of $CsCu_2Cl_3$ and $CsAg_2I_3$, *Acta Crystallographica*, **7**, 176–180.
18. A. Wells (1962) *Structural Inorganic Chemistry*, 3rd edn, Clarendon Press, Oxford, pp. 863–865.
19. M. Matecki and M. Poulain (1988) Cadmium and lead fluoride glasses, *Materials Science Forum*, **32–33**, 167–172.
20. A. Jha and J.M. Parker (1990) Formation of CdF_2 mixed halide glasses, *Physics and Chemistry of Glasses*.
21. M. Poulain, M. Poulain, J. Lucas, and P. Brun (1975) Halide glasses, *Materials Research Bulletin*, **10**, 243–245.
22. T. Grande, S. Aasland, and S. Julsrud (1992) Phase equilibria in the ZrF_4-BaF_2 glass-Forming system, *Journal of Non-Crystalline Solids*, **140**, 73–76.
23. T. Grande, S. Aasland, and S. Julsrud (1993) Thermodynamics of ZrF_4-BaF_2-NaF glass-forming system, *Journal of Non-Crystalline Solids*, **161**, 86–90.
24. G. Hatem, M. Gaune-Escard, and M. Hoch (1993) Experimental thermodynamics and phase equilibria estimation in Zr-fluoride glasses, *Journal of Non-Crystalline Solids* **161**, 91–97.
25. M. Poulain (1991) Fluoride glass composition and processing, in *Fluoride Glass Fibre Optics* (eds I.D. Aggarwal and G. Lu), Academic Press, San Diego, ch 1, pp. 1–33.
26. J.M. Parker (1990) Properties of fluoride glasses, in *Fluoride Glass Optical Fibres*, Blackie, Glasgow and London, ch 2, pp. 32–37.
27. W.H. Zachariasen (1932) *Journal of the American Chemical Society*, **54**, 3841.
28. R.L. Mozzi and B.E. Warren (1969) The structure of vitreous silica, *Journal of Applied Crystallography*, **2**, 164–172.
29. Wikipedia (2015) Pauling electronegativity, http://en.wikipedia.org/wiki/Electronegativity#Pauling_electronegativity.
30. K.H. Sun (1947) *Journal of the American Ceramic Society*, **30**, 277.
31. H. Rawson (1967) *Inorganic Glass-forming Systems*, Academic Press, London, ch 1.
32. J.H. Simmons, C.A. Simmons and R. Ochoa (1991) Fluoride glass structure in *Fluoride Glass Fibre Optics* (eds I.D. Aggarwal and G. Lu), Academic Press, London, ch 2, pp. 1–33.
33. Y. Al-Douri, H. Abid, and H. Aourag (2000) Some empirical formulas for calculating the ionicity character in semiconductors. *Materials Chemistry and Physics*, **65**, 117–119.
34. R.E. Cohen and co-workers (June 1988) *Physica C: Superconductivity*, **153–155**, Part 1, pp. 202–203.
35. C. Quintanar and co-workers (2003) *International Journal of Quantum Chemistry*, **96**, 483–491.
36. J.C. Phillips (1974) *Bonds and Bands in Semiconductors*, Academic Press, San Diego.
37. A.R. West (1988) *Basic Solid State Chemistry*, John Wiley & Sons Ltd, Chichester, pp. 86–92.

38. D. Liu, S. Zhang, and Z. Wu (2003) Lattice energy estimation for inorganic ionic crystals. *Inorganic Chemistry*, **42**, 2465–2469.
39. V.D. Zhuralev (2007) Calculation of the bond ionicity in complex oxides. *Bullettin of the Russian Academy of Sciences, Physics*, **71** (No. 5), 681–685.
40. A.F. Kapustinskii (1956) *Quarterly Review of Chemical Society*, **10**, 283.
41. Z.J. Wu and S.Y. Zhang (1999) Semiempirical method for the evaluation of bond covalency in complex crystals. *Journal of Physical Chemistry A*, **103**, 4270–4274.
42. J.C. Phillips (1979) Topology of covalent non-crystalline solids I: Short-range order in chalcogenide alloys. *Journal of Non-Crystalline Solids*, **34**, 153–181; J.C. Phillips (1981) Topology of covalent non-crystalline solids II: Medium-range order in chalcogenide alloys and amorphous Si (Ge). *Journal of Non-Crystalline Solids*, **43**, 37–77.
43. Wikipedia (2015) http://en.wikipedia.org/wiki/Orbital_hybridisation.
44. S. Hampshire (2008) Oxynitride glasses. *Journal of the European Ceramic Society*, **28**, 1475–1483.
45. K. Liddell, H. Mandal, D.P. Thompson (1997) X-ray data for new Y-Si-Al-O-N glass ceramics. *Journal of the European Ceramic Society*, **17**, 781–787.
46. M.M. Imon and S.H. Risbud (1986) Oxycarbonitride glass formation by melt solidification. *Journal of Materials Science Letters*, **5**, 397–398.
47. O.V. Mazurin, M.V. Streltsina, and T.P. Shvaiko-Shvaikovskaya (1991) *Handbook of Glass Data Part D*, Physical Sciences Data 15, Elsevier Science Publishers B. V., Amsterdam.
48. W.H. Dumbaugh (1986) Heavy metal oxide glasses containing Bi_2O_3. *Physics and Chemistry of Glasses*, **27**, 119–123.
49. J.E. Stanworth (1952) *Tellurite glasses*, **Nature**, **169**, 581–582
50. M. Imaoka and T. Yamazaki (1975) Reports from Institute of Industrial Science, *University of Tokyo*, **24** (2), 80. M Imaoka and T Yamazaki (1976) Reports from Institute of Industrial Science, *University of Tokyo*, **26** (1), 4.
51. Y. Dimitriev, V. Dimitrov and M. Arnaudov (1979) Infrared spectra of related ceramic phases and glasses in the TeO_2-V_2O_5-Me_2O system. *Journal of Materials Science*, **14**, 723–727.
52. Y. Dimitriev, I. Ivanova, and E. Gatev (1981) Glass-formation in binary vanadate systems. *Journal of Non-Crystalline Solids*, **45**, 297–300.
53. W. Vogel, H. Buerger, G. Zerge, W. Mueller, and K. Forkel (1974) *Silicattech*. **26** (6) 205.
54. C.M. Baldwin and J.D. Mackenzie (1979) Fundamental condition for glass formation in fluoride systems. *J American Ceramic Society*, **62**, 537–538.
55. C.A. Angell and J. Wong (1970) Structure and glass transition thermodynamics of liquid zinc chloride from far-infrared, Raman, and probe ion electronic and vibrational spectra. *Journal of Chemical Physics*, **53**, 2053–2066.
56. M. Poulain (1981) Glass formation in Ionic systems. *Nature*, **293**, 279–280.
57. M. Poulain, M. Poulain, and G. Maze (1980) *French Patent* 80.06088.
58. J. Lucas, H. Slim, and G. Fonteneau (1981) New fluoride glasses based on 4f and 5f elements. *Journal of Non-Crystalline Solids*, **44**, 31–35.
59. M. Poulain (1983) Halide glasses. *Journal of Non-Crystalline Solids*, **56**, 1–14.

60. M. Poulain, M. Poulain, and M. Matecki (1982) Rare earths in fluoride glasses: The LnF_3-AlF_3-ThF_4-BaF_2 systems and related glasses. *Journal of Non-Crystalline Solids*, **51**, 201–215.
61. K.H. Sun (1949) Fluoride glasses. *US Pat.* 2,466,509 (5-4-49).
62. J.J. Videau, J. Portier, and B. Piriou (1979) Sur de nouveaux verres aluminofluorés, *Revue de Chimie Minerale*, **16**, 393–399.
63. J.J. Videau, B. Dubois, and J. Portier (1983) Indium fluoride based glasses. *Competes Rendus de l'Academie des Sciences Paris*, **297**, 483–485.
64. T. Kanamori and S. Sakaguchi (1986) Preparation of elevated NA Fluoride optical fibers. *Japanese Journal of Applied Physics*, **25**, L468–470.
65. T. Izumitani and M. Tsutome (1977) *US Patent application US* 05/819,440.
66. A. Mazuki (2003) PhD Thesis on Neodymium-doped AlF_3 based Glasses for Waveguide Engineering, University of Leeds.
67. L. Santos, L.F. Santos, R.M. Almeida, V.K. Tikhomirov, and A. Jha (2001) Raman spectra and structure of fluoroaluminophosphate glasses. *Journal of Non-Crystalline Solids*, **284** (1–3), 43–48.
68. A. Mazuki and A. Jha (2007) Effect of Pb-ions on the kinetics of devitrification and viscosities of AlF_3-based glasses for waveguide fabrication. *Journal of Non-Crystalline Solids*, **353**, 1283–1286.
69. K.H. Jack (1976) Sialons and related nitrogen ceramics. *Journal of Materials Science*, **11**, 1135–1158.
70. G. Leng-Ward and M.H. Lewis (1989) Oxynitride glasses and their glass-ceramic derivatives, in *Glass and Glass Ceramics* (ed M. H. Lewis), 1st edn, Chapman & Hall, London, ch 4, pp. 106–153.
71. S. Hampshire, E. Nestor, R. Flynn, J.-L. Besson, T. Rouxel, L. Mercier, P. Goursat, M. Sebai, D.P. Thompson, and K. Liddell (1994) Yttrium oxynitride glasses: properties and potential for crystallisation to glass-ceramics oxynitride glasses. *Journal of the European Ceramic Society*, **14**, 261–273.
72. W.T. Young, L.K.L. Falk, H. Lemercier, V. Peltier-Baron, Y. Menke, and S. Hampshire (2000) The crystallization of the yttrium-sialon glass: $Y_{15.2}Si_{14.7}Al_{8.7}O_{54.1}N_{7.4}$. *Journal of Non-Crystalline Solids*, **270**, 6–19.
73. N.F. Mott (1977) Electrons in glass. *Contemporary Physics*, **18**, 225–245.
74. S.R. Ovshinsky (1968) Reversible electrical switching phenomena in disordered structures. *Physical Review Letters*, **21** (Issue 20), 1450–1453.
75. J. deNeufville, S.C. Moss, and S.R. Ovshinsky (1971) Rapid reversible light-induced crystallization of amorphous semiconductors. *Applied Physics Letters*, **18**, 254–257.
76. Z.U. Borisova (1981) *Glassy Semiconductors*, Plenum Press, New York, pp. 1–35.
77. P.N. Kumta and S.H. Risbud (1994) Rare-earth chalcogenides – an emerging class of optical materials. *Journal of Materials Science*, **29**, 1135–1158.
78. L. Cervinka and A. Hruby (1982) Structure of amorphous and glassy Sb_2S_3 and its connection with the structure of As_2X_3 arsenic chalcogenide glasses. *Journal of Non-Crystalline Solids*, **48**, 231–264.
79. A.M. Loireau-Lozac'h, M. Guittard, and J. Flahaut (1977) L_2S_3-Ga_2S_3 systems (L= La, Ce, Dy, Er and Y). *Materials Research Bulletin*, **12**, 881.

80. A. Wells (1962) *Structural Inorganic Chemistry*, 3rd edn, Clarendon Press, Oxford, pp. 464–467.
81. J. Heo and J.D. Mackenzie (1989) Chalcohalide glasses: synthesis and properties of Ge-S-Br and Ge-S-I glasses. *Journal of Non-Crystalline Solids*, **111**, 29–35.
82. S.A. Dembovskii, V.V. Kirilenko and Yu.A. Buslaev (1971) Vitrification in Ge-S-I system, *Izvestiya Akademii Nauk SSSR, Neorg, Materialy*, **7**, 328.
83. J.S. Sanghera, J. Heo, and J.D. Mackenzie (1988) Chalcohalide glasses, *Journal of Non-Crystalline Solids*, **103**, 155.